Xu Han, Wei Tian, Jim VanGilder, Wangda Zuo and Cary Faulkner (2020) An Open Source Fast Fluid Dynamics Model for Data Center Thermal Management. Energy and Buildings, DOI: https://doi.org/10.1016/j.enbuild.2020.110599

An Open Source Fast Fluid Dynamics Model for Data Center Thermal Management

Xu Han [a], Wei Tian [b], Jim VanGilder [b], Wangda Zuo [a,c*], Cary Faulkner [a]

[a] *Department of Civil, Environmental and Architectural Engineering, University of Colorado Boulder, UCB 428, Boulder, CO 80309, U.S.A.*

[b] *Schneider Electric, 800 Federal Street, Andover, MA 01810, U.S.A.*

[c] *National Renewable Energy National Laboratory, Golden, CO 80401. U.S.A.*

*Corresponding Author: Email: Wangda.Zuo@colorado.edu; Phone: 303-492-4333; Address: ECCE 247, UCB 428, 1111 Engineering Dr., Boulder, CO 80309

Abstract

Although computational fluid dynamics (CFD) has been widely adopted to improve data center thermal management, the high computational demand limits its applications, such as multivariate optimal design and operation. Fast fluid dynamics (FFD), which has been applied for fast airflow simulation, shows great potential. However, few research applied FFD for optimal design and operation of data center thermal management. This research improves the FFD model for data centers and conducts a comprehensive evaluation and demonstration. First, the FFD model is improved by solving the advection and diffusion equations together using an upwind scheme instead of a semi-Lagrangian advection solver in the conventional FFD. Second, new features for data centers are added, such as a pressure correction method to simulate plenum airflow and dynamic boundary conditions for IT racks. The new FFD model is first validated with two indoor environment cases and the results show that the new FFD model has slightly better overall prediction accuracy and faster speed compared to conventional FFD. It is also observed that both FFD models achieve acceptable accuracy, except for a few localized disparities with experimental data, which might be due to simplified handling of turbulence viscosity near the boundaries. Furthermore, validation with a real data center case shows that the FFD model achieves a similar level of accuracy as CFD when compared to the experimental measurements with some level of uncertainties. It is then demonstrated for data center optimal design and operation, which saves 53.4-58.8% of annual energy while still meeting the thermal requirements. With a much faster speed and comparable accuracy compared to CFD, the FFD model parallelized on a graphics processing unit is promising for practical model-based data center early design and operation.

Keywords: Data Center; Airflow and Thermal Management; Fast Fluid Dynamics; Model-Based Design and Operation.

1 Introduction

Data centers house a large amount of mission-critical IT equipment, such as IT servers, network and communication servers, and data storage devices, which dissipate effectively all input power as heat during operation. Data centers require cooling to remove the heat dissipated from the IT equipment to ensure the IT equipment operates reliably. It was reported that data centers consumed approximately 1.8% of the total U.S. electricity [1], with 24%-60% of this being consumed by the cooling system alone [2]. As the IT equipment becomes increasingly more power-intensive, it imposes more challenges on the data center cooling system [3]. As of today, air cooling is still the dominant method for primary heat removal from data centers, though liquid cooling is emerging as an energy-saving alternative [4].

Data center thermal management is crucial for reliable operation of IT equipment and energy efficiency of the cooling system in the data center, which typically involves non-uniform and complex airflow dynamics [5]. For example, medium and large-size data centers are usually configured with alternating cold aisles and hot aisles to ensure the IT rack inlet temperatures are within a safe threshold by eliminating or reducing the mixing of the cooling system supply cold air and IT rack exhaust hot air. However, many data centers are over-cooled, such as more cold air is supplied than needed, just to dilute a few local hot spots (i.e. locations at the intake of IT equipment where the measured temperature is greater than the recommended value), which leads to a low energy efficiency of the cooling system. Model-based design and operation methods can be adopted to improve the thermal management in data centers by evaluating the cooling performance for different scenarios. For example, in the design phase, the model can help determine the layout of IT racks, the open-area-ratio (ratio of open area to total area) and location of the perforated tiles, and the depth of the raised-floor plenum. In the operation phase, the model can help determine the optimal setpoints of the supply air flow rate and temperature to achieve the best energy performance while still meeting the thermal requirements of data centers.

To support model-based design and operation for data centers, many available thermal management models have been utilized with varying levels of complexity and accuracy. CFD was used to predict detailed airflow and temperature fields in the data center [6, 7]. Potential flow models [8] and linear abstract heat flow models [9] were also employed as fast prediction techniques. To further accelerate the speed of predictions, artificial neural networks [10] and reduced order models (e.g. Proper Orthogonal Decomposition) [11] were utilized to obtain some critical information of the data center thermal environment. Among these methods, CFD has been widely used as a more sophisticated method than others. A recent study showed that, with careful calibration, CFD can make reliable predictions of perforated-tile air flow rates and rack-inlet temperatures [12]. However, while versatile and generally accurate, CFD is computationally expensive (especially when the size of the data center is large). This makes its use in optimal design and operation of data centers difficult, especially when multiple parameters are optimized, which requires a large number of simulations.

Conventional CFD commonly employs the Semi-Implicit Method for Pressure Linked Equations (SIMPLE) [13] to solve the governing equations for fluid flow. For simplicity, the conventional CFD is referred to as CFD in the rest of the paper. To accelerate CFD, an alternative CFD model called fast fluid dynamics (FFD) was proposed and applied to predict indoor environment. FFD solves the same set of governing equations as CFD, but with a time-split method and semi-Lagrangian advection solver. FFD was reported to be 50 times faster than CFD and it can additionally speedup 30 times by running in parallel on graphics processing unit (GPU) [14, 15]. This level of speed improvement has great potential to significantly accelerate the process of model-based design and operation for data centers. FFD was first introduced and verified in building simulation applications by Zuo and Chen [16]. FFD was then improved to simulate different cases such as indoor airflow [14, 15, 17], airflow around buildings [18], cabin environment [19], and urban-scale airflows [20]. However, the airflow and thermal dynamics in data centers are quite different compared to these applications [5]. One is that the high thermal load and airflow rate make the airflow pattern in the data center more complex than that in regular indoor environment. The other is that special treatments for boundary conditions unique for data centers are needed, such as perforated floor tiles and IT racks with server fans inside. Some previous studies [12, 21, 22] tried to use FFD for data center airflow and thermal modeling and showed potential, but these studies lack a comprehensive evaluation of using FFD for optimal design and operation of data center thermal management. In addition, the FFD programs implemented in those studies are proprietary. This research develops the necessary FFD modules for data center and conducts a comprehensive evaluation of FFD for that regarding prediction accuracy, computing speed and performance for model-based design and operation in a real data center. The new FFD model for data center thermal management is implemented using OpenCL, which is a cross-platform parallel computing language. To enable the large-scale application, the FFD code has been publicly released under a free open-source license.

This paper is organized as follows. First, a comprehensive introduction of the new FFD model is provided including governing equations, methods to solve these equations, treatments of special boundary conditions in data centers and their implementation. The new FFD model is validated with two classical cases for indoor environment modeling [23] in Section 3.1 and a real data center case located in Massachusetts, U.S.A in Section 3.2. Subsequently, the application of the FFD model is demonstrated using three case studies based on the aforementioned data center.

2 Methodology

2.1 Data Center Airflow and Thermal Dynamics

The configuration and intended airflow directions of a typical raised-floor data center are shown in Figure 1. The above-floor white space (i.e. allocated for IT equipment) in the data center is partitioned into cold aisles and hot aisles by rows of racks. The raised-floor plenum and perforated floor tiles are designed to uniformly distribute the cold air to the cold aisles. The cold air from the

cooling system is supplied to the cold aisle, then flows through the IT racks and carries heat dissipated from IT equipment, and then exhausts to the hot aisle and returns to the cooling system through the ceiling plenum. ASHRAE [24] defines the requirements of the data center airflow and thermal management. One key parameter is to ensure the rack inlet temperatures are within a safe threshold (e.g. not exceeding 27 ^{o}C). The segregated cold and hot aisles help lower the IT rack inlet temperature by preventing or mitigating the mixing of cold and hot air. Sometimes, physical containment of the hot or cold aisle is employed to avoid such mixing.

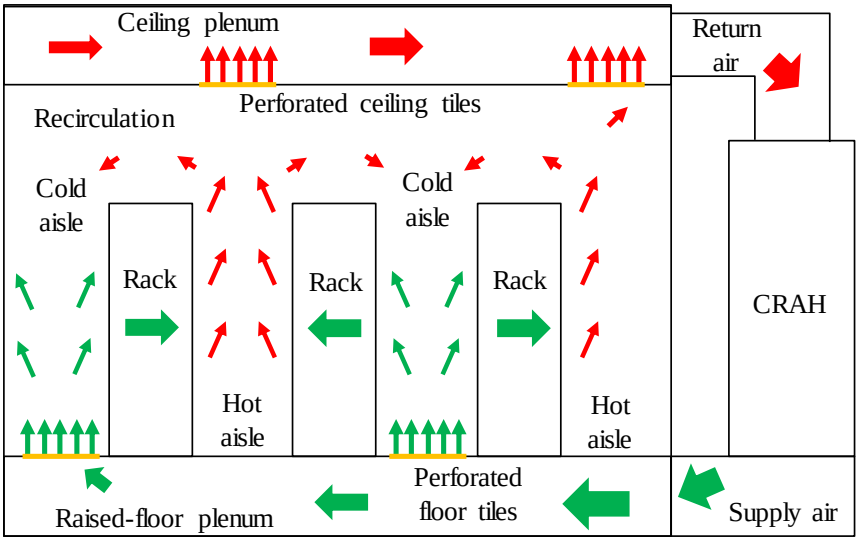

Figure 1 Airflow pattern in a typical raised-floor data center

CFD has been widely used to improve the data center thermal management. For example, CFD can be adopted to evaluate the temperature and airflow distribution for scenarios with different designs, such as different layouts of the cold aisle, hot aisle and IT racks. However, one limitation of CFD is the high computational demand, which makes its application infeasible when multiple parameters are studied and hundreds or even thousands of simulations are needed. Thus, the FFD model, which was reported to be 50 times faster than CFD [15], is evaluated in this paper to solve this problem.

2.2 Fast Fluid Dynamics

This section introduces conventional FFD for indoor environment modeling and the improved FFD model for data center thermal management. Note that here the "conventional FFD" represents existing FFD [12, 15, 25-27] as opposed to the proposed FFD described later in this paper. The improvements include changing the solving methods for the advection equation and implementing boundary conditions and special treatments for data center environment. The implementation of the FFD model in OpenCL is also discussed.

2.2.1 Governing Equations and Solution Methods

Like CFD, the FFD model solves the same set of governing equations for flows. The Navier-Stokes momentum equation can be generalized and written as:

$$\frac{\partial \boldsymbol{U}_i}{\partial t} = -\boldsymbol{U}_j \frac{\partial \boldsymbol{U}_i}{\partial \boldsymbol{x}_j} + \nu \frac{\partial^2 \boldsymbol{U}_i}{\partial \boldsymbol{x}_j \partial \boldsymbol{x}_j} - \frac{1}{\rho}\frac{\partial P}{\partial \boldsymbol{x}_i} + \boldsymbol{F}_i, \quad (1)$$

where $\boldsymbol{U}$ is the velocity vector, t is time, $\boldsymbol{x}$ is the spatial coordinates, ν is the kinematic viscosity, ρ is the density, P is pressure, and $\boldsymbol{F}_i$ is the source term.

The energy equation can be written as:

$$\frac{\partial T}{\partial t} = -\boldsymbol{U}_j \frac{\partial T}{\partial \boldsymbol{x}_j} + \alpha \frac{\partial^2 T}{\partial \boldsymbol{x}_j \partial \boldsymbol{x}_j} + \boldsymbol{S}_T, \quad (2)$$

where T is the temperature, α is the thermal diffusivity, and $\boldsymbol{S}_T$ is the thermal source term.

FFD uses a time-split method. Equation 1, for example, is split into three equations in conventional FFD [15]:

$$\frac{U_i^{(1)} - U_i^{(n)}}{\Delta t} = -\boldsymbol{U}_j \frac{\partial \boldsymbol{U}_i}{\partial \boldsymbol{x}_j}, \quad (3)$$

$$\frac{U_i^{(2)} - U_i^{(1)}}{\Delta t} = \nu \frac{\partial^2 \boldsymbol{U}_i}{\partial \boldsymbol{x}_j \partial \boldsymbol{x}_j} + \boldsymbol{F}_i, \quad (4)$$

$$\frac{U_i^{(n+1)} - U_i^{(2)}}{\Delta t} = -\frac{1}{\rho}\frac{\partial P}{\partial \boldsymbol{x}_i}. \quad (5)$$

The three equations are solved sequentially. As shown in Figure 2, conventional FFD first solves Equation (3), namely the advection equation, by a semi-Lagrangian (SL) scheme [28]. Equation (4), namely the diffusion equation, is solved with an implicit scheme. Finally, Equation (5), namely the pressure equation, is solved together with the continuity equation:

$$\frac{\partial \boldsymbol{U}_i}{\partial \boldsymbol{x}_i} = 0, \tag{6}$$

based on a projection-correction method [29] to ensure mass conservation.

The SL scheme [28] has been widely adopted to solve the advection equation in conventional FFD [14, 15, 17-20]. One of the major advantages of the SL scheme is the fast computing speed, which is achieved by tracing locations at the last time step and calculating velocities through interpolation without any iterative algorithm. However, a major drawback of the SL scheme is that it does not guarantee in-general quantity conservation [30]. In addition, the determination of the time step size is crucial for the stability of simulation as well as the accuracy of the SL scheme [31]. For example, the Courant–Friedrichs–Lewy (CFL) constraints ($\boldsymbol{U}_i \Delta t/\Delta x \leq 1$) should be satisfied to overcome the stability concerns, which may require a small time-step size. Meanwhile, a smaller time step size may also reduce accuracy because of truncation error growth [31]. As a result, additional efforts are required to address these issues. On the other hand, an implicit scheme, such as the first order upwind, is stable and robust even when the CFL number is larger than one. However, the implicit scheme is usually more computationally expensive compared to the SL scheme. Thus, it will increase the computing demand by 8%-20% according to our tests if the SL scheme is replaced by an implicit scheme to solve the advection equation.

In addition to the stability and robustness, the first order upwind scheme has another advantage compared to the SL scheme, which is the unconditional conservation of mass and energy for each cell in the computational domain. With SL, one will have to enforce mass balance at the global level. Even by doing so, the mass balance at cell level is not perfect. This is particularly important in data center applications, because unlike regular buildings where the purpose is to create an environment with general thermal comfort, data center operators and researchers care more about local energy balance, which may influence the generations of local hot spots.

To take advantage of the stability, robustness and unconditional local mass and energy conservation of the first order upwind scheme while not sacrificing computing speed, this paper proposes a new FFD model to simultaneously solve diffusion and advection equations with a first order upwind scheme (Figure 2). The Equations (3) and (4) are solved together as:

$$\frac{U_i^{(2)} - U_i^{(n)}}{\Delta t} = \nu \frac{\partial^2 \boldsymbol{U}_i}{\partial \boldsymbol{x}_j \partial \boldsymbol{x}_j} + \boldsymbol{F}_i - \boldsymbol{U}_j \frac{\partial \boldsymbol{U}_i}{\partial \boldsymbol{x}_j}, \tag{7}$$

For clarity, the proposed FFD model is called FFD-Upwind (or the FFD model) and the conventional FFD model is called FFD-SL. As shown in Figure 2, the FFD-Upwind first assigns coefficients of equation matrix for diffusion and advection sequentially and then solve the equation

matrix with a linear Gauss-Seidel (GS) or Jacobi solver. As a result, the FFD-Upwind discards the SL scheme without increasing the computing demand compared to the FFD-SL.

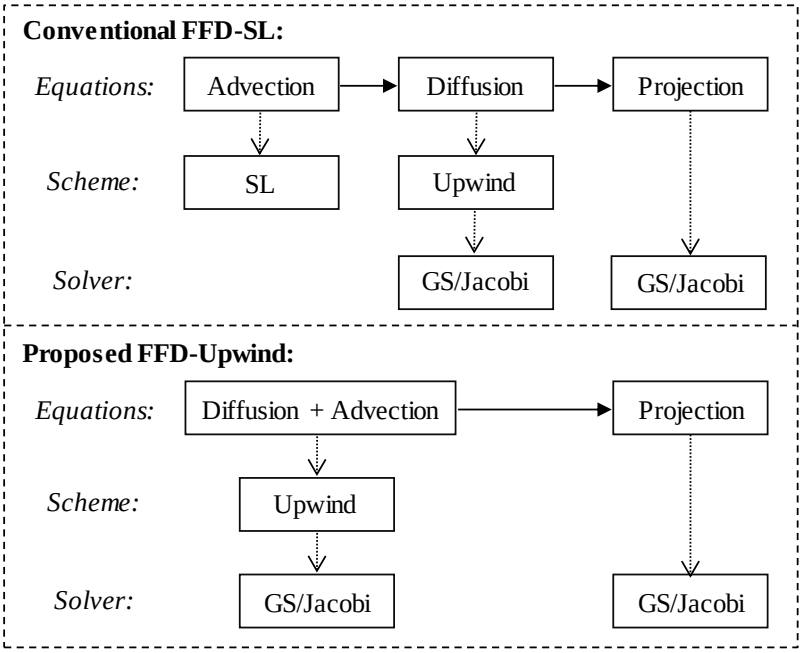

Figure 2 Workflow of the convectional FFD-SL and proposed FFD-Upwind

2.1.2 Boundary conditions

In this section the general boundary conditions that are commonly used for modeling of indoor environment are briefly introduced. The special boundary conditions for objects in the data center environment are then described including perforated floor tiles and IT racks.

General boundary conditions:

In our study, three general types of boundaries are considered including inlets, outlets, and walls. A Dirichlet boundary condition is applied for the inlets as a fixed velocity. For the outlets, either a Neumann boundary condition with a zero-gradient velocity or a Dirichlet boundary condition with a fixed velocity can be imposed. For the walls, a no-slip wall boundary condition is applied, which assumes the air velocity at the solid wall boundary is zero.

Perforated floor tile:

Since the raised-floor plenum and white space are modeled separately in this paper, the modeling of perforated floor tiles can be done with different considerations depending on which space is studied [5]. The aim of modeling the raised-floor plenum is to predict the air flow rates at perforated tiles. The flow rates are determined by the pressure distribution in the plenum and the pressure drop when the air flows through the perforated tiles. We adopt a commonly used approach

called the porous jump method (also regarded as lumped resistance method). It simplifies the perforated tiles as flow resistances and specifies a step pressure loss across the perforated tiles [5, 7, 32]:

$$\Delta P = \frac{1}{2}\rho f V^2, \tag{8}$$

where ΔP is the pressure drop across the tile, V is the velocity approaching the tile, and f is the dimensionless loss coefficient, which can be estimated from manufacturer data or by empirical formulae, for example, the one proposed by Fried and Idelchik [33]:

$$f = \frac{1}{\beta^2}[1 + 0.5(1-\beta)^{0.75} + 1.414(1-\beta)^{0.375}], \tag{9}$$

where β is the open-area-ratio of the perforated tile.

When modeling the white space, the goal is to study the airflow and temperature distribution within the space. The perforated tiles are just special inlet boundary conditions. As a result, they are often treated as prescribed uniform-velocity boundaries independent of their open-area-ratio. The magnitude of the velocity is typically determined based on the air flow rate and the total area of the perforated tile. However, in reality, the airflow will be accelerated when it goes through the small openings of the perforated tiles, which results in higher local velocities and a lower-pressure region above the perforated tiles.

Balancing the complexity and accuracy of modeling such perforated tiles should be considered. On one hand, modeling the perforated tiles as fully opened openings with a pressure loss using the porous jump model would omit the jet effect above the tiles, and therefore may lead to inaccurate or even incorrect results [32]. On the other hand, detailed pore-by-pore modeling, although versatile and generally accurate, is impractical in practice considering the added complexity. Consequently, there are various attempts in this area to achieve a compromise between complexity and accuracy of modeling the perforated tiles. The body force model or modified body force model were used to specify a momentum source above the perforated tiles [32, 34]. Abdelmaksoud, et al. [34] also developed a quadrants method, which separates the perforated tile to multiple openings with the same total opening area. All these methods were reported to successfully capture the air acceleration through the pores of the perforated tiles. This research adopts the body force method [32] due to its simplicity and good accuracy. An additional force is added into the momentum equations to correct the under-estimated velocity for computational cells just above the perforated floor tiles. Suppose that a perforated tile has an open-area-ratio of β, surface area A (m^2) and air

flow rate Q (m^3/s). With the assumption that the momentum source is applied to a computational cell with a height h (m) directly above the tile, we can compute the momentum source as:

$$\boldsymbol{F}_i = \frac{Q^2}{A^2 h}\left(\frac{1}{\beta} - 1\right), \tag{10}$$

where the direction of $\boldsymbol{F}_i$ is perpendicular to the surface orientation of the perforated tile. In this paper, we set h as 0.15 m.

IT Rack:

There are generally two approaches to model the IT racks: the open box model and the black box model [35]. The major difference between the two methods is that the airflow inside the rack is modeled in the open box model but is excluded in the black box model. The former method adopts a more detailed model, which may be able to capture the temperature and velocity stratification across the surfaces of the rack inlet and outlet. The latter method simplifies the rack as a solid box with an inlet and an outlet. The exhaust temperature at the rack outlet is calculated based on the temperature profile of the air flowing into the rack inlet, with an assumed temperature rise to model the effect of heat dissipation inside the rack. Zhang, et al. [36] compared different levels of details for modeling an IT rack including a black box rack, a detailed rack with crude server simulators and a detailed rack with detailed server simulators, and found that the different levels of rack details had little effect on the predicted temperatures for the studied case. Therefore, in the present study, we adopt the black box model for its simplicity and sufficient prediction performance. In the black-box model, individual servers or "slices" are not explicitly resolved. The airflow is assumed to be proportional to total rack power dissipation (P, kW) with 212 m^3/h (125 cfm) of airflow for each kW of power (ψ, $m^3/h/kW$) [12, 37]. The airflow is spread uniformly over the front and rear of the rack.

$$Q_{in} = P \times \psi \tag{11}$$

The air temperature at the rack inlet is assigned with the temperature of its adjacent cells. The vertical temperature gradient at the front (inlet) of the rack is carried through to the rear (exhaust) of the rack with a temperature rise, which is determined by the heat dissipation of IT servers and flow rate of air through the rack:

$$T_{ex} = T_{in} + \frac{q_{server}}{c_p \times \dot{m}} \tag{12}$$

2.1.3 Software Implementation

The data center can be split into two volumes: the raised-floor plenum and white space [5]. A previous study [38] recommended to model the raised-floor plenum separately and use the results of flow rates at perforated tiles as boundary conditions in the white space model. For modeling convenience, our current implementation follows the procedure of modeling the raised-floor plenum and the white space separately. This is justified when relatively low open-area-ratio tiles are employed.

The structure and workflow of the FFD model is shown in Figure 3. The FFD model is implemented through hybrid programming in C and OpenCL. The host program (i.e. main routine of FFD) runs sequentially on the CPU and the kernels run in parallel on the GPU. The code in OpenCL is used to execute the kernels for assigning boundary conditions and solving the governing equations. For more details of the structure of the implementation, please refer to Tian, et al. [17]. It is noted that the source codes of this FFD model have been publicly released in [39] , which is the first open source FFD model for data center thermal management.

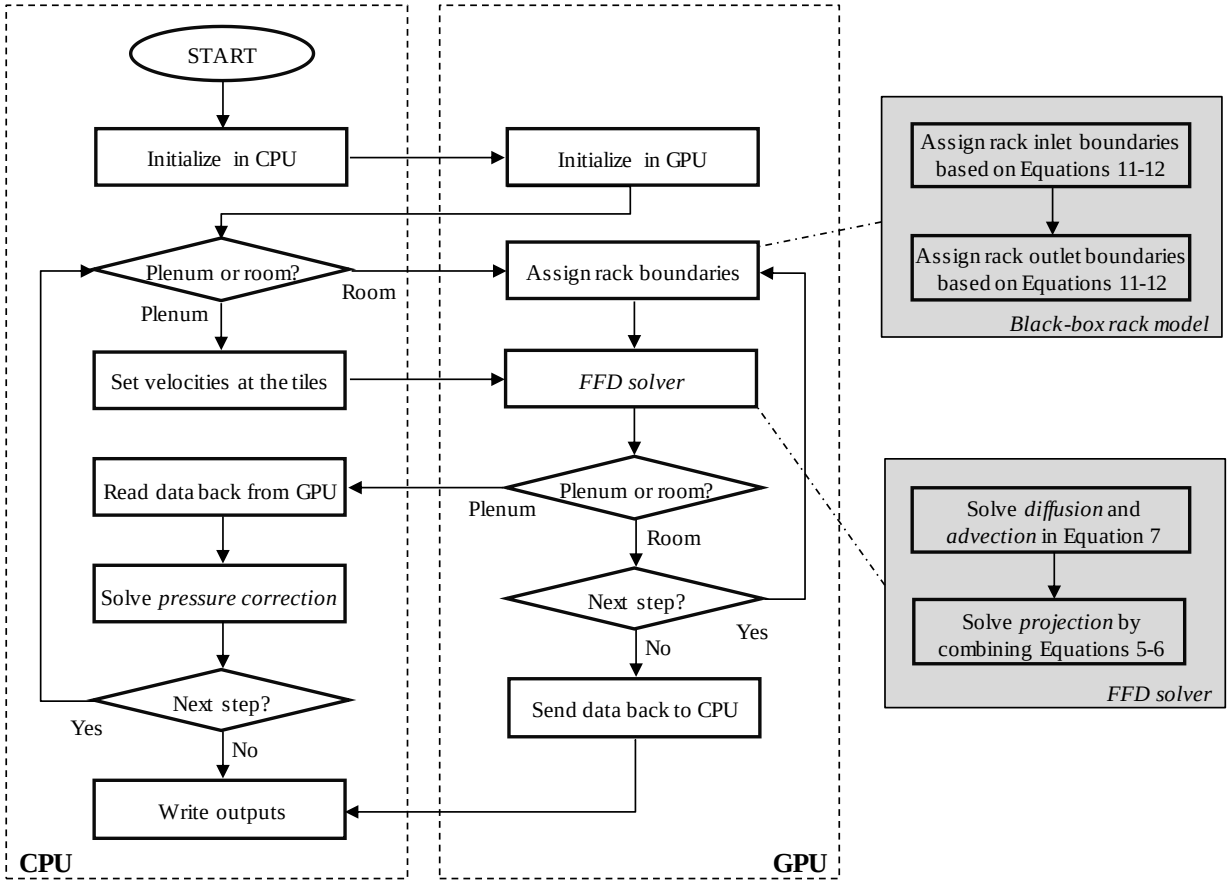

Figure 3 Structure of the proposed FFD model

When modeling the raised-floor plenum, to ensure that the simulated airflow field and air flow rates at tiles simultaneously satisfy Equations (1) and (7), we adopt a pressure correction method proposed by VanGilder, et al. [40]. The FFD first assigns initial values for all air flow rates at tiles and computes the pressure field in the raised floor plenum based on Equation (5) and (6). The FFD model then calculates the air flow rates at tiles according to the obtained pressure field and Equation (7) and checks the mass conservation. Subsequently, the FFD model shifts the pressure in the plenum by a constant value (for example, the pressure at all cells in the plenum will be increased by a constant value if the current pressure field is too small to provide enough outflows) until a converged flow field satisfying momentum and mass conservation is achieved.

When modeling the white space, we adopt a black box model to assign the boundary conditions for the IT racks based on Equations 10 and 11 [12]. All the governing equations are solved based on a Jacobi method on the GPU in parallel. For the modeling of both plenum and white space, the simulation will be terminated when the velocity, temperature and pressure fields become steady state.

3 Validation

To validate the proposed FFD model, two classic cases for indoor environment modeling and one data center case are selected. The indoor cases are studied to evaluate the proposed FFD model that solves the advection and diffusion equations together, compared to conventional FFD that solves them separately. The real data center case is then studied to evaluate the capability of the proposed FFD model with new features to simulate data center thermal environment. Experimental data are taken as reference for all the cases.

3.1 Validation of the Improved FFD Model

3.1.1 Description of the indoor environment cases

The first case is an empty room with forced convection, which is a pure airflow case without heat transfer [23]. The room is 2.44 m (8 ft) long, 2.44 m (8 ft) wide and 2.44 m (8 ft) high with an inlet at the top of the west wall and an outlet at the bottom of the east wall. Other critical dimensions are shown in Figure 4 (a). The temperatures of the inlet flow and surfaces in the room are controlled to be the same. Experimental data at ten locations as shown in Figure 4 (b) are available [23].

The second case increases the flow complexity by adding a heated box (1.22 m × 1.22 m × 1.22 m) in the center of the room, in which heat transfer occurs [23]. The size of room and locations of the inlet and outlet are the same with the first case. Other critical dimensions are shown in Figure 5 (a). The temperatures of the inlet flow, box surface, ceiling, flow and other walls are 22.2 ºC., 36.7 ºC, 25.8 ºC, 26.9 ºC, and 27.4 ºC, respectively. Experimental data is available for ten locations shown in Figure 5 (b) [23].

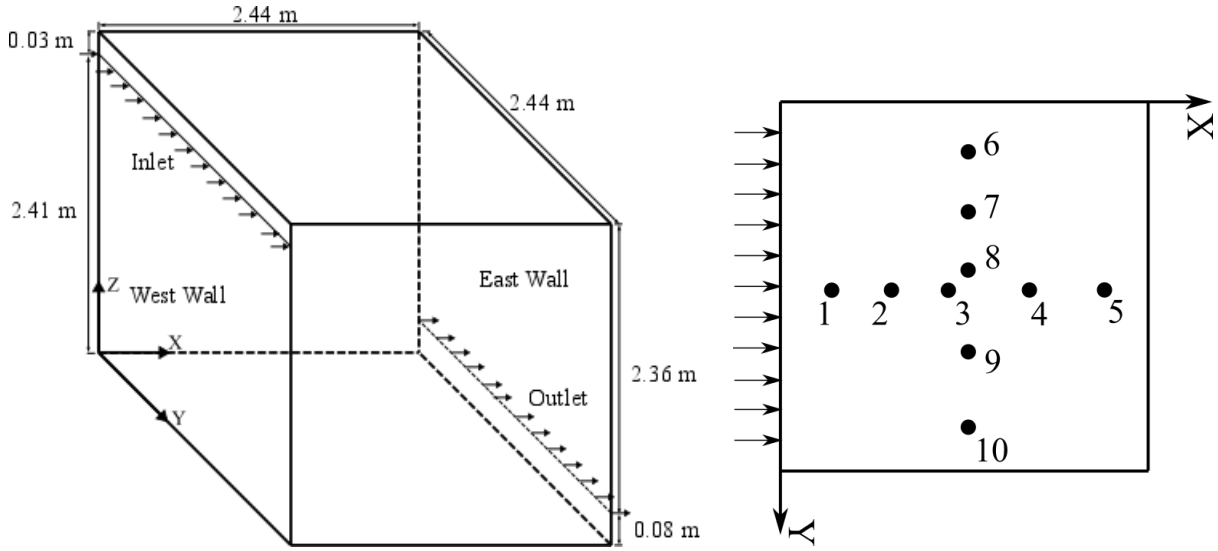

(a) (b)

Figure 4 (a) Schematic of the forced convection in an empty room and (b) locations of experimental data

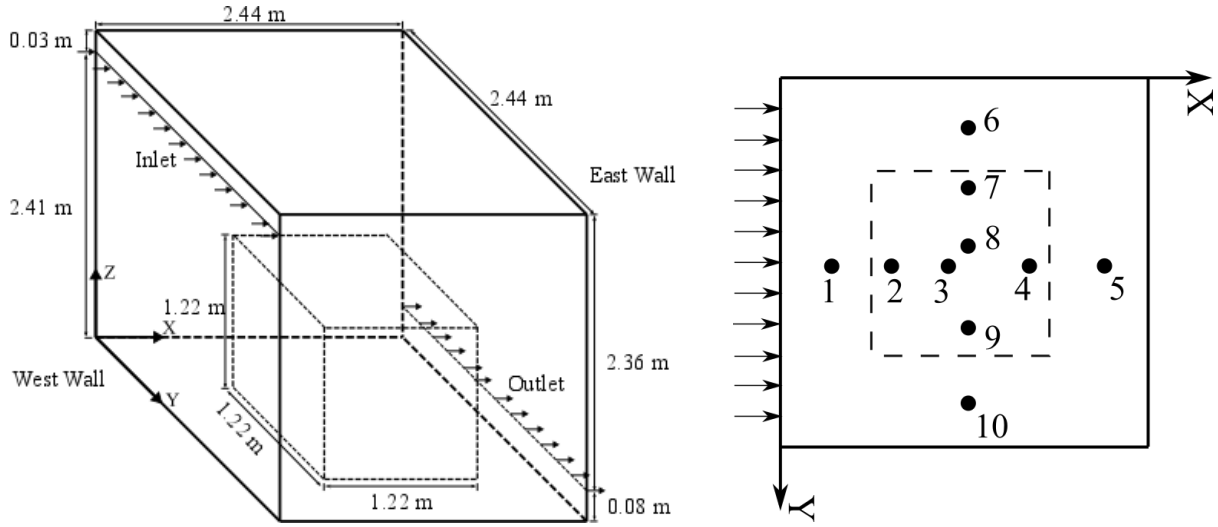

(a) (b)

Figure 5 (a) Schematic of the mixed convection in a room with a box and (b) locations of experimental data

3.1.2 Evaluation metrics

Normalized root-mean-square deviation (NRMSD) is adopted to quantify the accuracy of predictions by FFD and CFD with respect to experimental data, which is defined as:

$$NRMSD = \frac{1}{x_{max}-x_{min}}\sqrt{\frac{\sum_{i=1}^{N}(\hat{x}_i - x_i)^2}{N}} \times 100\%, \quad (13)$$

where $\hat{x}_i$ and x_i are simulated and measured values at point i, respectively. N is the total number of data points. $(x_{max} - x_{\min})$ represents the range of the studied parameter over the computational domain, which is 1.36 m/s when evaluating velocity profiles and 14.5 ºC (36.7 ºC - 22.2 ºC) when evaluating temperature profiles for the two cases.

3.1.3 Setup of simulations

Table 1 Settings of simulations in FFD-Upwind and FFD-SL

Case	**Grid**		**Simulation Time (s)**		**Time Step Size (s)**	
	FFD-Upwind	FFD-SL	FFD-Upwind	FFD-SL	FFD-Upwind	FFD-SL
Forced Convection in an Empty Room	40×40×40		1350		0.05	
Mixed Convection in a Room with a Box	40×40×40		1350		0.05	

Table 1 summarizes the simulation settings employed in both FFD-Upwind and FFD-SL. We perform a similar grid independent study as was done in Tian, et al. [17]. It is found that with the non-uniform structured grid (40×40×40), in which the averaged mesh size is about 6 cm, the simulations achieve grid independent results. Similar conclusions were drawn in previous studies [17, 23]. The mesh is refined at critical locations to capture the gradients and changes in the flow. For example, the inlet as well as near-ceiling areas is refined with a minimum mesh size of about 0.5 cm and the outlet as well as the near-floor area is refined with a minimum mesh size of about 1 cm. The FFD-Upwind and FFD-SL models perform transient-state simulations because of the time-split method used in FFD (with a time step size of 0.05 s and simulation time of 1350 s). Both FFD-Upwind and FFD-SL use a zero-equation turbulence model [41, 42] and are performed on an AMD FirePro^{TM} W8100 GPU.

3.1.4 Results

Table 2 summarizes the NRMSD of predictions for the cases with FFD-Upwind and FFD-SL. The average NRMSDs for the four locations with FFD-Upwind are 5.18% and 4% for the two cases. The FFD-Upwind has slightly better overall prediction accuracy with lower averaged NRMSDs for the two cases compared to FFD-SL. However, it can still be seen that FFD-SL performs better than FFD-Upwind for velocity predictions at the locations P1 and P5. This may be due to the complex flow structure in those areas, which is hard to capture.

Table 2 NRMSD of predictions for cases with FFD-Upwind and FFD-SL

Cases	Simulation Program	Predictions	NRMSD (%)				
			P1	P3	P5	P6	Ave.
Forced Convection in an Empty Room	FFD-SL	Velocity	3.72	7.95	6.59	8.56	6.71
	FFD-Upwind	Velocity	4.93	4.25	6.93	4.62	5.18
Mixed Convection in a Room with a Box	FFD-SL	Velocity	5.22	5.46	4.18	4.38	5.25
		Temperature	5.44	6.68	2.84	7.78	
	FFD-Upwind	Velocity	6.92	4.21	7.19	3.47	4.00
		Temperature	2.33	3.47	2.43	1.99	

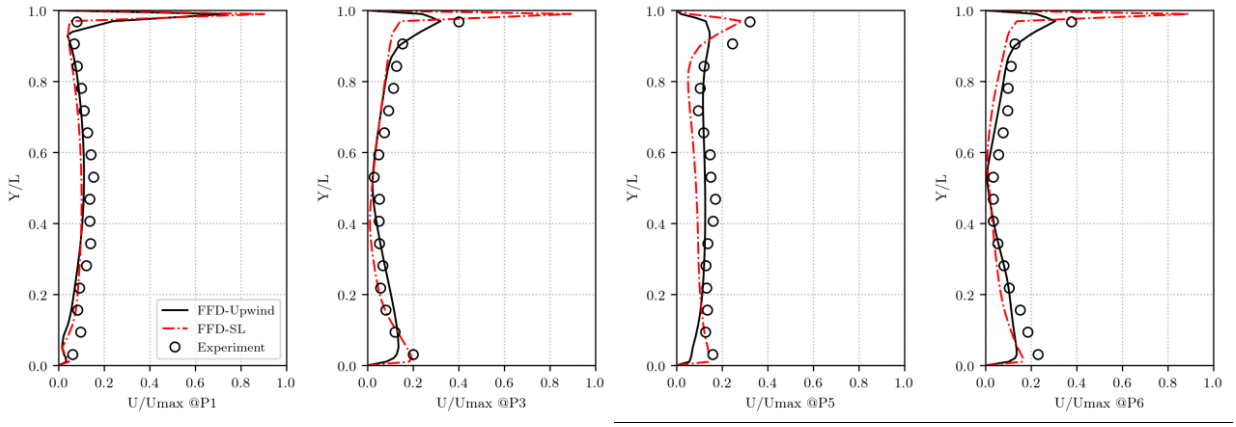

Figure 6 Comparison of velocity profiles for forced convection in an empty room

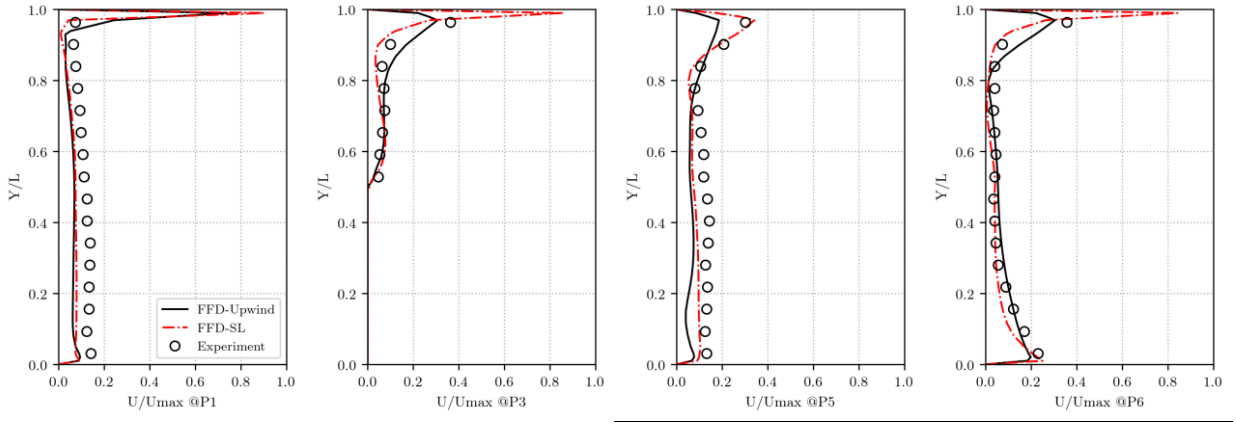

Figure 7 Comparison of velocity profiles for mixed convection in an empty room with a box

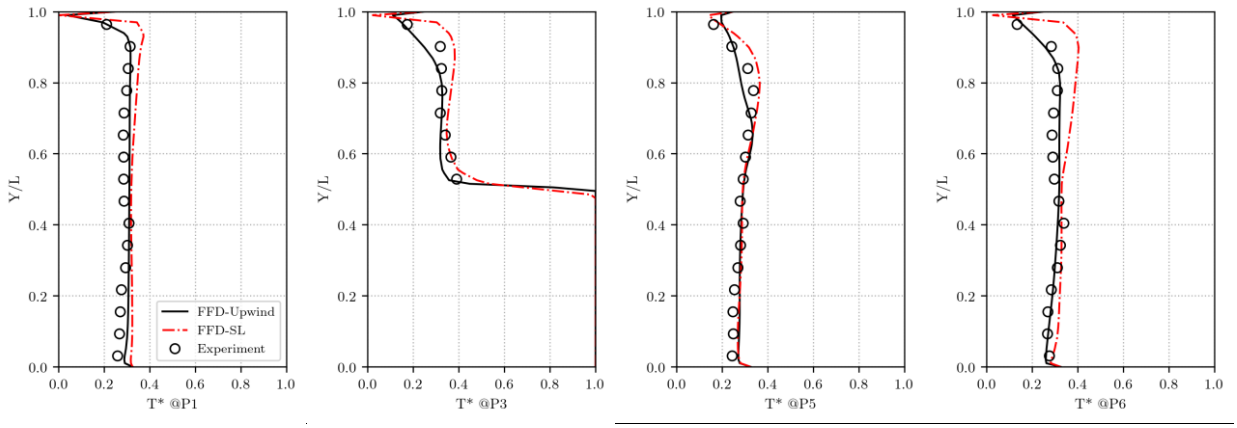

Figure 8 Comparison of temperature profiles for mixed convection in an empty room with a box

Figure 6-8 compare the velocity and temperature profiles predicted by FFD-Upwind and FFD-SL for the two cases. Generally, all agree with the experimental data [23] for most locations and FFD-Upwind performs slightly better than FFD-SL does. However, some obvious discrepancies can be observed. For example, velocity prediction at P5 by FFD-Upwind and temperature prediction at P6 by FFD-SL for the second case. Both FFD-Upwind and FFD-SL do not predict the velocity at the areas close to the ceiling and floor precisely. The possible reason is that FFD could not properly estimate the turbulence viscosity due to lack of wall functions even though an approximate wall function [42] is integrated with the zero-equation turbulence model in the FFD models. It is also found that FFD-SL performs better than FFD-Upwind at those areas especially for the location P5 even though FFD-Upwind has a slightly better overall accuracy. This is possible since the prediction accuracy may be influenced by aspects other than the solving methods of FFD, such as configurations of the mesh, settings of physical parameters. It is worthy to note that relatively larger discrepancies in some critical areas were also found in previous studies [25, 43] and even state-of-the-art CFD models with advanced turbulence models could not precisely predict all the flow details [23]. As a simplified alternative to CFD models that targets fast speed, it is acceptable that the proposed FFD model could generally capture the flow dynamics.

For the speed, it takes 244.1 s and 244.9 s for the two cases with FFD-Upwind and takes 260.3 s and 258.0 s for the two cases with FFD-SL. This is because of the new methods to solve equations in the FFD-Upwind as shown in Figure 2. In FFD-SL, the advection equation is solved with an SL scheme and the diffusion equation is solved with an upwind scheme. In FFD-Upwind, the advection and diffusion equations are solved together with an upwind scheme. As a result, the computing demand in FFD-Upwind is reduced by eliminating the SL scheme. Hence, FFD-Upwind is faster than FFD-SL. To conclude, FFD-Upwind is about 5.7% faster than FFD-SL while achieving a slightly better overall accuracy compared to FFD-SL for the two studied cases.

3.2 Validation of New Features for Data Centers

Section 2.1.2-2.1.3 introduced the new features in the FFD model for data centers. This section is to validate the new FFD model using a real data center for industrial practice. It is noted that various research has been done to validate the component models for data centers, such as the black box model [35, 36] and body force method [32]. The focus of this paper is to evaluate if the new FFD model can provide airflow prediction for real-world practice with the current implementation, such as zero-equation turbulence model, body force model and black box rack model. Therefore, we select a middle-size data center in real world instead of a simple data center with well-controlled boundary conditions in the laboratory.

3.2.1 Description of the data center case

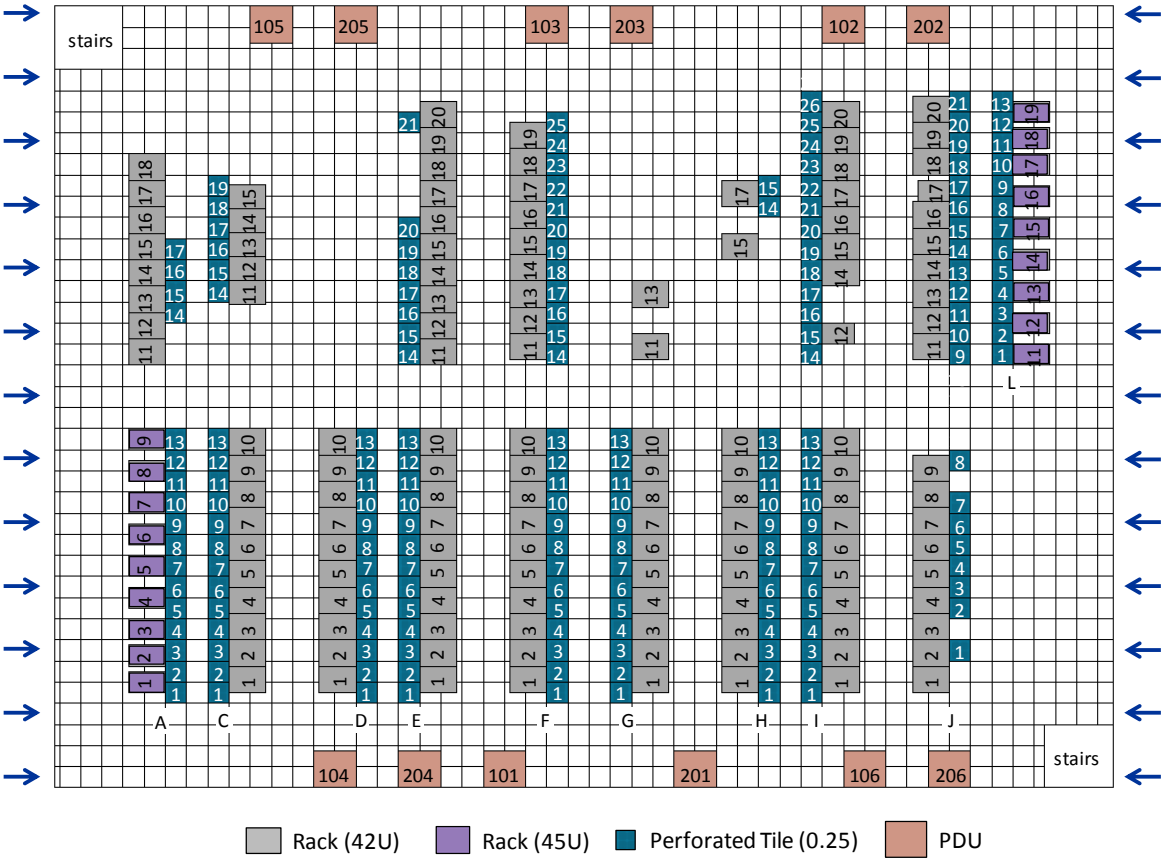

Figure 9 Layout of the reference data center

In this section, the new FFD model with the new data center feature is validated using a real medium-size data center with raised-floor and dropped-ceiling architecture located in Massachusetts, U.S.A. As shown in Figure 9, the reference data center is approximately 30.5 m (100 ft) long, 22.6 m (74 ft) wide and 3.4 m (11 ft) high from the raised floor to the ceiling, with a total white space area of approximately 690 m^2 (7,400 ft^2). Total power consumption by 151

racks and 12 PDUs is approximately 344 kW. Racks G11 and G13 (i.e., the 11th and 12th cabinets in Row G) are empty. There are 18 45U networking racks in Rows 1 and 10, and all the remaining racks in the data center have a capacity of 42U.

Two central Air Handling Units (AHUs) supply cooling airflow through the short sides of the plenum, which is supported using 7/8" stanchions. The total supply air flow rate is 152,000 m^3/hr (89200 cfm). The airflow is then supplied to the IT equipment through 183 perforated floor tiles with 25% open-area-ratio (each 2 ft by 2 ft). The hot exhaust air returns to the CRAH through a dropped-ceiling plenum with 42 perforated ceiling tiles with 83% open-area-ratio.

An on-site measurement was performed for the studied data center. In addition to the data center geometry and types of IT racks, three primary parameters are measured including 1) rack-by-rack powers, 2) perforated tile airflow rates and 3) rack inlet temperatures. Rack-by-rack powers are estimated by two steps. First, all the racks fed by twelve large power distribution units (PDUs) are divided into twelve groups and the total power of each group is equal to the corresponding PDU power. Then, rack-by-rack powers are estimated by scaling the total power in each group of racks by the fraction of occupied U spaces in each rack. A flow hood is used to measure the perforated tile airflow rates. The flow hood is a TSI/Alnor EBT731 and the accuracy of the flow hood is ±3% of reading and ±12 m^3/h at flows >85 m^3/h. When being placed on a perforated tile, the flow hood adds additional flow resistance which creates a measurement error relative to the true value. To correct for this error, the "2MUP(p=2)" method proposed by VanGilder, et al. [44] is adopted. The rack inlet temperatures are measured at 4 points distributed vertically in front of each rack. The sensors are located at heights of 0.53 m, 0.91 m, 1.3 m and 1.68 m, respectively. The horizontal distance between the thermocouples and the rack door is approximately 0.025 m. Four K-type thermocouples are connected to a UEi-DT304 Quad Input IP67 Digital Logging Thermometer with the accuracy of ±[0.1% + 0.5 °C]. Temperature measurements are averaged over a 1-minute sampling period.

3.2.2 Evaluation metrics

To evaluate accuracy of plenum airflow modeling we propose the percentage relative difference (PRD) between simulated tile airflow $\dot{Q}_{sim}$ and experimentally measured tile airflow $\dot{Q}_{exp}$, which is defined as:

$$PRD_{\dot{Q}} = \left|\frac{\dot{Q}_{sim}-\dot{Q}_{exp}}{\dot{Q}_{exp}}\right| \times 100\%. \quad (14)$$

To evaluate accuracy of temperature prediction in the white space, PRD_T is used to represent the PRD between simulated and experimentally measured rack inlet temperatures (T_{sim} and T_{exp}):

$$PRD_T = \left|\frac{T_{sim} - T_{exp}}{\Delta T}\right| \times 100\%, \quad (15)$$

where T_{sim} and T_{exp} are calculated as the average of the temperature at four points along the heights. The reference temperature difference ΔT is assumed to be 14 °C (25 °F), which corresponds to a typical magnitude of temperature rise across the racks. In this case, a 5% of PRD_T corresponds to a temperature difference of 0.7 °C.

3.2.3 Setup of simulations

Table 3 summarizes the simulation settings of the FFD model and CFD. Both use structured grids for the simulation of plenum and white space. The CFD does not require a time step size or a set simulation time since it performs steady-state simulations, while the FFD model performs transient-state simulations because of the time-split method used in FFD (with a time step size of 0.2 s – 1.0 s and simulation time of 100s – 400s). The CFD uses a $k - \varepsilon$ turbulence model with wall function treatment while the FFD model uses a zero-equation turbulence model [41] with a simplified approximate-wall-function proposed by Dhoot, et al. [42]. The CFD simulation is performed on four cores of an Intel (R) Xeon (R) CPU E3-1220 v6 processor running on a Windows workstation with 32 GB of RAM. The FFD simulation is performed on an AMD FirePro™ W8100 GPU. Except for the refined cells at some critical locations to handle complex geometries, a uniform and structured grid with the mesh size of 0.15 m (6 inches) is adopted for this case in both the FFD and CFD models. The grid independent studies show that the results do not change significantly when the mesh size is below 0.15 m (6 inches) in both models. Similar conclusions were drawn in VanGilder and Zhang [45], which studied ten data center layouts with six grid levels each.

Table 3 Settings of simulations in FFD and CFD

Case	**Grid**		**Simulation Time (s)**		**Time Step Size (s)**	
	FFD	CFD	FFD	CFD	FFD	CFD
Plenum	224×161×6	224×161×6	100	N/A	1.0	N/A
White space	200×148×22	200×148×22	400		0.2	

FFD and CFD models use the same settings for the boundary conditions. The walls are assumed to be adiabatic since the heat dissipation from the IT equipment is much larger than the heat flux through walls. The leakage is neglected in the CFD/FFD models as the total raised floor leakage airflow for this data center is negligible according to Pardey, et al. [37]. In the plenum model, the inlet bays are modeled with Dirichlet boundary conditions and the velocities are assigned with measured data. The outlet, i.e. floor perforated tiles, are modeled as two-dimensional flow resistances. In the whitespace model, the perforated tiles become inlets, which are modeled with Dirichlet boundary conditions with air flow rates and temperatures equal to the measurements. An

additional momentum force is added to the cells above the floor perforated tiles to correct the under-estimated velocity due to the usage of fully-opened openings to model the perforated inlets in the CFD and FFD models. The outlets of the whitespace, i.e. ceiling perforated tiles, are simplified with fixed flow. The IT racks are modeled as a "black box" [35]. The server flow rates are assumed to be 125 cfm/kW [37]. The server powers are assigned based on the on-site audit results of the rack-by-rack powers.

It is noteworthy that the dropped-ceiling plenum is excluded from the FFD and CFD modeling for modeling convenience and simplicity. We perform CFD simulations to determine the effect of removing the ceiling plenum and find that the temperatures at the rack inlets are not affected. The perforated ceiling tiles are treated as fixed-flow outlets. In the plenum models, the measured supply air flow rates at all side inlets are used as model inputs. In white space models, the measured flow rates and temperatures at perforated floor tiles are used as model inputs.

3.2.4 Results

The results of the plenum simulation are depicted in Figure 10. The predictions of air flow rates through the 183 perforated tiles in the reference data center by FFD and CFD are categorized by PRD from experimentally measured data. Both FFD and CFD has 95.1% of their predictions with a PRD less than 5% from the experimental measurements. Only 7 (3.8%) predictions from FFD and 8 (4.4%) predictions from CFD are within the PRD of 10-20% from experimental measurements. There are only two predictions (1.1%) from FFD and one prediction (0.55%) from CFD with deviation of more than 20% from the experimental measurements.

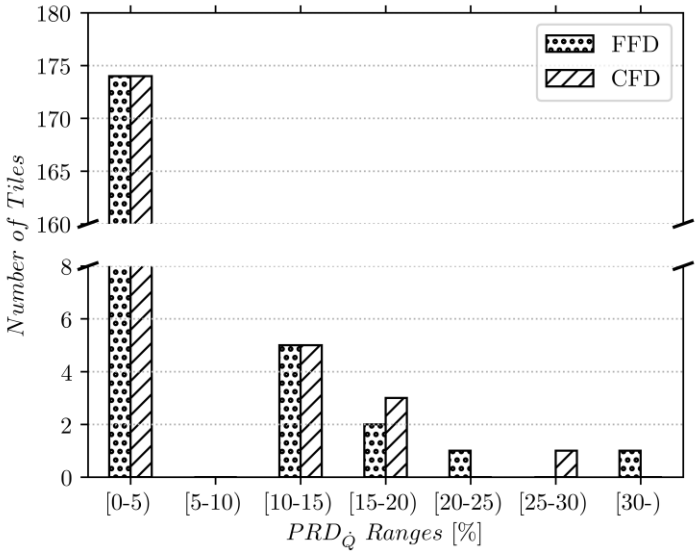

Figure 10 Predictions of perforated-tile air flow rates categorized by percentage relative difference (PRD) from measurements

The results of the white space simulations are shown in Figure 11. The predictions of rack-inlet temperatures at 149 racks (excluding 2 empty racks) in the reference data center by FFD and CFD are categorized by PRD from experimental measurements. 131 (88.0%) predictions from FFD and 128 (85.9%) predictions from CFD deviate by less than 10% from the experimental measurements. 14 (9.4%) predictions from FFD and 16 (10.7%) predictions from CFD are within the 10%-to-20% relative difference range from experimental measurements. 4 (2.7%) predictions from FFD and 5 (3.4%) predictions from CFD deviate by more than 20% from the experimental measurements.

Generally, both FFD and CFD capture the rack-to-rack inlet temperature variation well. However, some discrepancies between simulated and measured temperatures can be observed for both FFD and CFD. The reasons may be as follows. First, the dynamic changing of the cooling system might affect the measured air flow rates and temperatures at perforated tiles, given the measurement usually takes several hours. Second, we did not have all required information about this real data center for the models, such as the leakage path through openings in or under the rack or floor cracks. Moreover, some assumptions in the FFD and CFD models might not be able to represent the real situation. For instance, individual-rack power consumption is crudely estimated based on rack IT population and power measurements from PDUs, which served many racks. The rack airflow is, in turn, crudely estimated to be 212 m^3/h (125 cfm) of airflow for each kW of power dissipation. Furthermore, additional uncertainties may also lie in the measurements since it is very hard to perfectly measure a real data center in operation, which was discussed in [44]. Even so, both FFD and CFD successfully predict the inlet temperature for more than 85% of the racks with a less-than-10% error. To conclude, the proposed FFD model achieves a similar level of sufficient accuracy compared to CFD for the studied case.

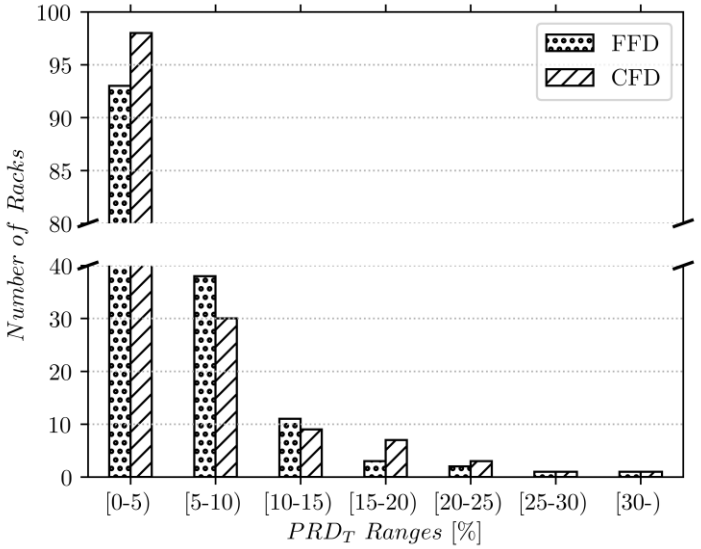

Figure 11 Predictions of rack-inlet temperatures categorized by percentage relative difference (PRD) from measurements

For the simulation speed, CFD takes 10.3 minutes and 65.6 minutes while FFD takes 0.17 minutes and 1.07 minutes to simulate the raised-floor plenum and white space, respectively. FFD is approximately 61 times faster compared to CFD. It is noted that the present solution time is obtained based on the current settings of the models for the reference data center and computer configurations. CFD runs on four cores of CPU while FFD runs on a GPU in parallel.

4 Case Studies

In this section, the usage of FFD model for data center design and operation is demonstrated by applying it to improve data center thermal management through model-based design and operation. These include 1) an optimal design of data center plenum and perforated tiles; 2) an optimal design of the data center cooling system regarding fan sizing and designed supply air temperature through parametric studies; 3) an optimal operation of the cooling system by optimizing setpoints of supply air flow rate and temperature based on the weather conditions.

4.1 Optimal Design of the Plenum and Perforated Tiles

The design of a data center normally involves the determination of several key parameters, such as layout of the IT racks, width of cold aisles and hot aisles, plenum depth and perforated tile open-area-ratio.

In the early design stage, the decision should be made based on the cooling performance, initial cost and operational cost. The initial cost could be roughly estimated using existing database and engineering experience, but it is usually hard to get the quantitative evaluation of the cooling performance and operational cost. CFD has been widely used to do that, but it is limited to evaluating a few scenarios instead of a systematic parametric study of multiple parameters due to its high computational demand.

In this case, we demonstrate the usage of the FFD model for the optimal design of data centers, in which the effect of the design of plenum and perforated tile on the air distribution uniformity is investigated.

4.1.1 Evaluation metrics

A real data center can have hundreds of perforated tiles or more. Here we assume the design purpose is to uniformly distribute air flow to perforated tiles. To evaluate the uniformity of the airflow distribution among many perforated tiles, we propose a percentage relative difference from the mean air flow rate of all perforated tiles:

$$PRD_{i,\dot{m}} = \frac{\dot{m}_i - \bar{\dot{m}}}{\bar{\dot{m}}} 100\%, \tag{16}$$

where $\dot{m}^i$ is the mass flow rates at perforated tiles *i*. The *n* is the total number of perforated tiles. $PRD_{\dot{m}}^i$ represents the percentage relative difference from the mean air flow rate of all perforated tiles at the perforated tile *i*. Ideally, if the cold air is distributed uniformly to each perforated tile, the $PRD_{\bar{m}}^i$ at all perforated tiles should be 0%. If the distribution is non-uniform, we can quantify the non-uniformity by evaluating the values and distribution of $PRD_{\dot{m}}^i$ of all perforated tiles.

4.1.2 Setup of the case

Table 4 Parameter settings in the case for optimal design of the plenum and perforated tiles

Parameters	**Unit**	**Values**
Plenum depth	mm	305, 457, 610, 762, 914
Tile open-area-ratio	%	15, 25, 35, 45, 56

As shown in Table 4, the studied parameters include the plenum depth and perforated tile open-area-ratio. The plenum depth ranges from 305 mm to 914 mm with an interval of 52 mm. The perforated tile open-area-ratio ranges from 15% to 56%. Among them 25% and 56% are commonly used in practice and the others are selected with an interval of 10%. As a result, there are a total of 25 cases for the parametric study. All other parameters are determined based on the operational data. The supply air temperature is 22 ^{o}C, which is calculated by averaging measured supply air temperatures. The supply air flow rate is 1.5×10^5 m^3/h, which corresponds to an air ratio of 2.07 calculated based in Equation 17. The air ratio is defined as the ratio of total supply air flowrate ($\dot{Q}_{sup}$) over total IT flowrate ($\dot{Q}_{in}$, refer to Equation 11):

$$Air\ Ratio = \frac{\dot{Q}_{sup}}{\dot{Q}_{in}} \tag{17}$$

4.1.3 Results

The results from parametric study are shown in Figure 12. The distribution of the $PRD_{\dot{m}}^i$ for all perforated tiles is depicted including maximum, minimum values and standard deviation. Generally, a greater plenum depth helps improve the airflow uniformity. The influence is more pronounced when the plenum depth is smaller than 610 mm. In terms of the open-area-ratio of perforated tiles, a smaller open-area-ratio helps improve the airflow uniformity. Once again, the influence is more significant when the plenum depth is smaller than 610 mm. The reason is that a deeper plenum and/or more restrictive perforated tiles can lead to a more uniform pressure distribution in the plenum. When the depth of plenum is larger than 610 mm, the pressure distribution in the plenum is already fairly uniform, so further improvement for both parameters may not help as much compared to the cases with a smaller plenum depth. Assuming the design objectives are that maximum and minimum values of $PRD_{\dot{m}}^i$ are smaller than 3% and the standard

deviation of PRD_m^i is smaller than 1%, the candidate combinations of tile open-area-ratio and plenum depth towards optimal design include 1) 15% + 457 mm and 2) 25% + 610 mm.

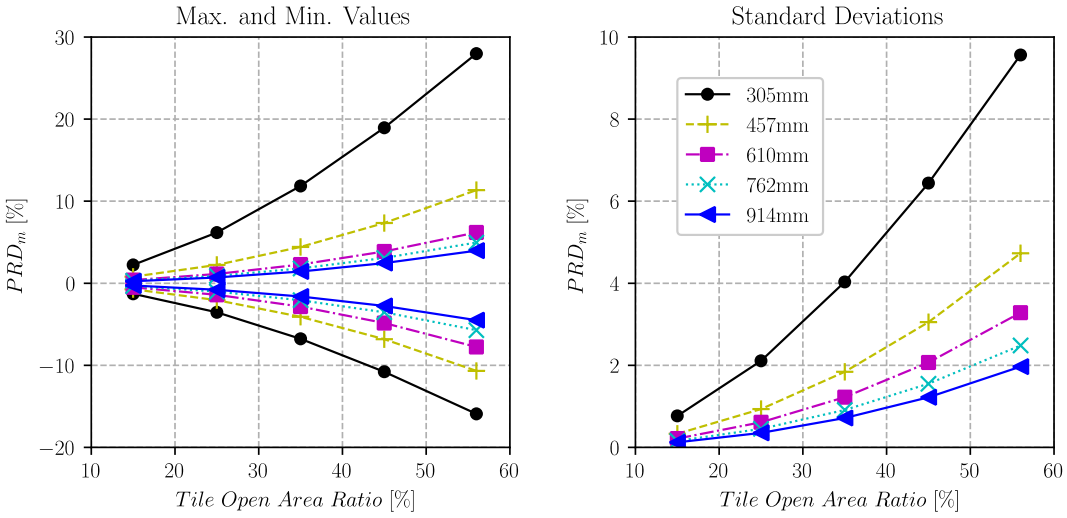

Figure 12 Effect of open-area-ratio of perforated tiles and plenum depth on airflow uniformity among perforated tiles

It is worth to point out that the decision in real world could be more complex. Although the airflow uniformity can be improved, a greater plenum depth may increase the capital cost of construction and a smaller open-area-ratio of perforated tiles may increase the operational cost due to a larger pressure drop through the tiles, which increases fan energy consumption. The fan energy can be estimated based on the flow rate and fan head pressure so that the operational cost for fan can be calculated. Therefore, the optimal design should balance the costs and performance. Such a parametric study in the early design stage using FFD simulations could provide quantitative suggestions towards an optimal design.

4.2 Optimal Design of the Data Center Cooling System

The previous sections demonstrated optimal design of the data center plenum and perforated tiles using the FFD model. This section demonstrates another optimal design use case of the FFD model, which is the optimal design of the cooling system in the same data center. This is done through a parametric study using FFD simulations, in which we focus on two parameters: fan sizing and designed supply air temperature.

4.2.1 Evaluation metrics

There are various metrics to evaluate the thermal environment of a data center, such as rack cooling index (RCI) [46], return temperature index (RTI) [47], supply heat index (SHI) and return heat index (RHI) [48] and capture index (CI) [49]. Among them we adopt the RCI [46], which

quantifies the conformance with the data center thermal standards, e.g. ASHRAE thermal guidelines [24], based on the calculation of equipment intake temperatures. ASHRAE guideline categorizes data centers into multiple classes and recommends different thermal standards for different classes. The data center we studied is Class A, which has tightly controlled thermal environment and mission critical operations. The RCI metric consists of two numbers: RCI_{HI} and RCI_{LO}. The RCI_{HI} can be written as:

$$RCI_{HI} = \left[1 - \frac{\sum_{x=1}^{n} f(x)}{n(T_{max-all} - T_{max-rec})}\right] 100\%, \tag{18}$$

$$f(x) = \begin{cases} T_x - T_{max-rec}; & T_x > T_{max-rec} \\ 0; & T_x \leq T_{max-rec} \end{cases}, \tag{19}$$

where, T_x is the mean rack-inlet temperature at Rack x; n is the total number of racks; $T_{max-rec}$ is the maximum recommended rack-inlet temperature (27 ^{o}C by [24]); $T_{max-all}$ is the maximum allowable rack-inlet temperature (35 ^{o}C by [24]). $RCI_{HI} = 100\%$ means no equipment intake temperature exceeds the maximum recommended value. The data center thermal environment can be regarded as "Good" when RCI_{HI} is larger than 96% and "Acceptable" when RCI_{HI} is in the 91%-to-95% range.

The RCI_{LO} can be written as:

$$RCI_{LO} = \left[1 - \frac{\sum_{x=1}^{n} g(x)}{n(T_{min-rec} - T_{min-all})}\right] 100\%, \tag{20}$$

$$g(x) = \begin{cases} T_{min-rec} - T_x; & T_x < T_{min-rec} \\ 0; & T_x \geq T_{min-rec} \end{cases}, \tag{21}$$

where, $T_{min-rec}$ is the minimum recommended rack-inlet temperature, which is 18 ^{o}C per ASHRAE [24]. $T_{min-all}$ is the minimum allowable rack-inlet temperature, which is 15 ^{o}C for Class A1 data centers per ASHRAE guideline. $RCI_{LO} = 100\%$ means no equipment intake temperature falls below the minimum recommended value (i.e. 18 ^{o}C per ASHRAE [24]). The data center thermal environment can be regarded as "Good" when RCI_{LO} is larger than 96% and "Acceptable" when RCI_{LO} is in the 91%-to-95% range.

Another metric used in our study is the maximum rack-inlet temperature, which can be written as:

$$T_{in}^{max} = \max_{x \in [1,n]} T_{in}^{x}, \quad (22)$$

where, T_{in}^{max} is the maximum rack-inlet temperature; T_{in}^{x} is the intake temperature at Rack x. The limit of T_{in}^{max} can be the maximum allowable rack-inlet temperature, which is 32 °C for Class A1 data centers per ASHRAE guideline. Other limits of T_{in}^{max} can also be adopted, e.g. 27 °C according to the requirement of the data center.

4.2.2 Setup of the case

Table 5 Parameter settings in the case for optimal design of the cooling system

Parameters	**Unit**	**Values**
Supply air temperature	°C	15, 16, 17, 18, 19, 20, 21, 22, 23, 24
Supply air flow rate	m^3/h	3.65×10^4, 5.5×10^4, 7.3×10^4, 9.1×10^4, 1.1×10^5, 1.28×10^5, 1.46×10^5, 1.51×10^5
	Air ratio	0.5, 0.75, 1.0, 1.25, 1.5, 1.75, 2.0, 2.07

The settings of parameters for this case are shown in Table 5. The supply air temperature ranges from 15 °C to 24 °C with a 1 °C interval. We define the air ratio ranging from 0.5 to 2.07. Therefore, there are 80 cases in total for the parametric study. It is noted that the air ratio of 2.07 is determined based on the current settings in the reference data center. Accordingly, the supply air flow rates are calculated for the prescribed air ratios. All other parameters are set according to current configurations in the reference data center.

4.2.3 Results

The effect of the two studied parameters on the cooling performance is investigated regarding three metrics including RCI_{LO}, RCI_{HI} and T_{in}^{max}. As shown in Figure 13 (a), when the air ratio is smaller than 1.25, RCI_{HI} increases as the air ratio increases. When the air ratio is greater than 1.25, RCI_{HI} stays constant at 1.0. Figure 13(b) shows the effect on the RCI_{LO}. For cases with supply air temperature from 15 to 17 °C, RCI_{LO} starts from a constant value of 1.0 when the air ratio is smaller than 0.75 and then falls drastically when the air ratio is larger than 1.0. For other cases, RCI_{LO} stays constant as the air ratio increases. The obvious turning points for both RCI_{HI} and RCI_{LO} start when the air ratio is around 1.0. As shown in Figure 13(c), the T_{in}^{max} decreases as the air ratio increases. The curves under different supply air temperature follow a similar pattern, which become relatively constant when the air ratio is larger than 1.25. The maximum rack-inlet temperatures when reaching constant values are higher than the supply air temperatures by approximately 3 °C.

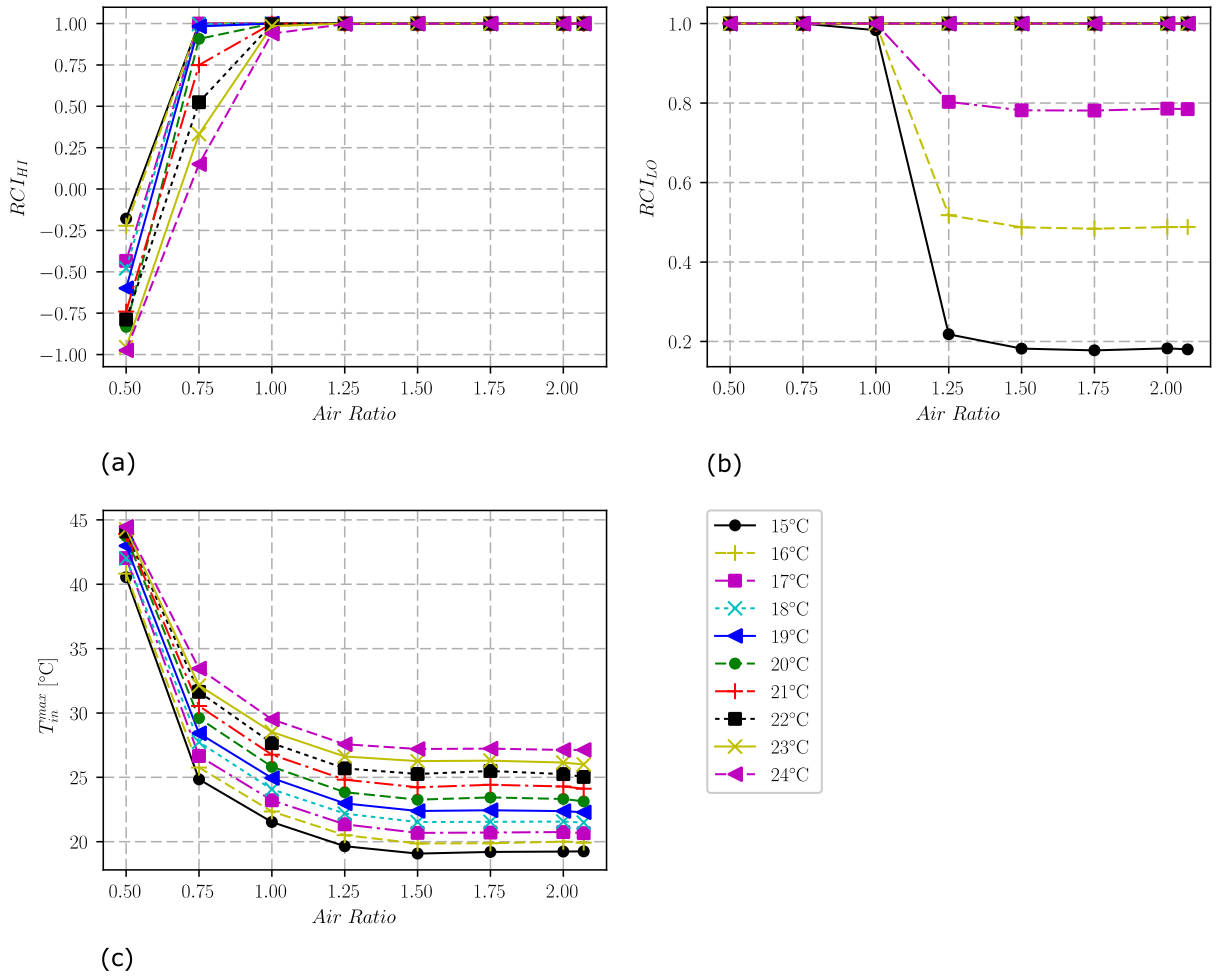

Figure 13 Effect of air ratio and supply air temperature on RCI_{LO}, RCI_{HI} and T_{in}^{max}

The maximum rack-inlet temperatures are generated at some critical locations, such as Rack-A17 and Rack-A18 (see their locations in Figure 9), where the cold supply air coming into the racks is richly mixed with hot room air due to lack of perforated tiles close to the racks. The temperature contours at 2/3-RACK height for different air ratios with supply air temperature of 16 ºC are plotted in Figure 14. When the air ratio is less than 1.0, the cooling system supplies less cold air than required by the IT equipment (i.e. total IT server air flow rate), causing recirculation (i.e. mixing cold supply air with hot room air) in front of racks. As a result, the rack-inlet temperatures are higher than the supply air temperature and local hot spots occur if the supply air temperature is not adequately cold. Interestingly, the RCI_{HI} values are negative when the air ratio is 0.5. According to Equations 18 and 19, the RCI_{HI} will be equal to 0 when the inlet temperatures at all racks are the maximum allowable equipment intake temperature (32 ºC).

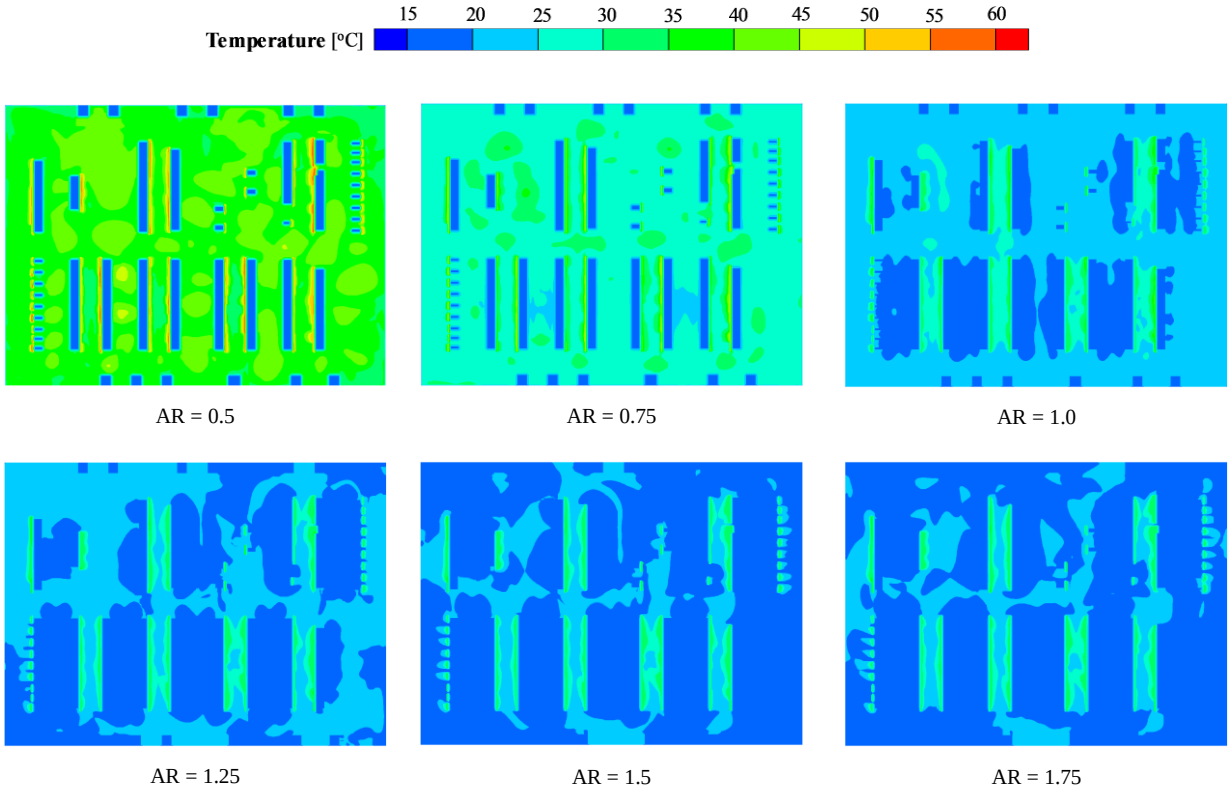

Figure 14 Temperature contours at 2/3-RACK height for different air ratios with supply air temperature of 16 °C

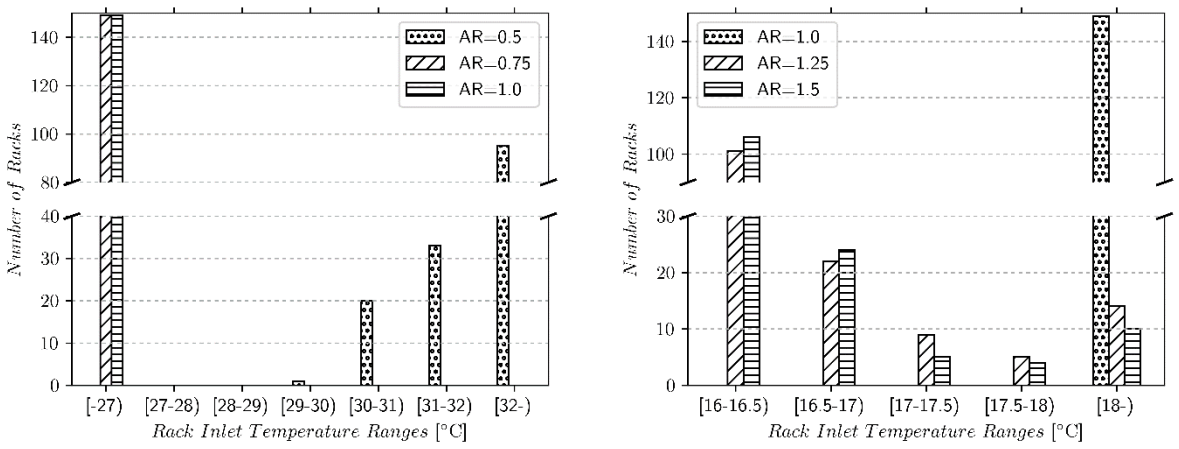

Figure 15 Number of racks with rack inlet temperature of different ranges for different air ratios with supply air temperature of 16 °C

The numbers of racks with inlet temperatures in different ranges are shown in Figure 15. We find that 95 (63.8%) racks have inlet temperatures higher than 32 °C and 53 (35.6%) racks have inlet

temperatures in the 30-32 ºC range when the air ratio is 0.5, which may lead to the negative value of RCI_{HI}. To conclude, the less cold air the cooling system supplies or the higher the supply air temperature is, the more local hot spots exist and the smaller the RCI_{HI} will be.

When the air ratio continues to increase after 1.0, the rack-inlet temperatures approach closer to the supply air temperature. Therefore, the RCI_{HI} stays constant as 1.0, and RCI_{LO} falls drastically after the air ratio increases past 1.0. This effect is more significant when the supply air temperature is lower. When the supply air temperature is higher than 18 ºC, the RCI_{LO} stays constant at 1.0 as the air ratio increases. When the supply temperature is lower than 18 ºC, the values of RCI_{LO} stay at 0.2, 0.5, and 0.8 for supply air temperatures of 15 ºC, 16 ºC, and 17 ºC, respectively. Take the case with supply air temperature of 16 ºC as an example. Ideally, the rack inlet temperatures should be close to the supply air temperature when the supply air flow rate is large enough. The RCI_{LO} should be equal to 0.33 according to Equations 17 and 18 if the rack inlet temperatures approach close to the supply air temperature. However, there are still several racks with inlet air largely mixed with hot room air. For example, for the case with air ratio of 1.5, there are 10 racks with inlet temperatures that are larger than 18 ºC (shown in Figure 15) including Racks A-11~12, A-16~18, E17~19, H-15 and J-01, which do not have perforated tiles close to them (see Figure 14 and Figure 9). There are 33 racks with inlet temperatures that are in 16.5-to-18.0 ºC range, such as Racks C-11, E-11 and J-2~3, which are located at the edge of each row or have relatively less cold air supply (see Figure 14 and Figure 9). As a result, the RCI_{LO} is determined to be 0.5 instead of 0.33.

From the results of the parametric study, the optimal air ratio that balances thermal environment and fan energy ranges from 1.25 to 1.5, which corresponds to the fan sizing from 9.1×10^4 to 1.1×10^5 m^3/h. The corresponding optimal designed supply air temperature should be between 20 and 21 ºC to create a similar thermal environment as baseline. Please note that there are multiple choices for the two studied parameters to create a similar thermal environment regarding the three metrics, but the real optimal design should be determined through considering other aspects, such as the energy efficiency of the cooling system.

4.3 Optimal Operation of the Data Center Cooling System

Other than optimal design of the cooling system, which considers a typical design condition, in this case, we demonstrate using the results of the parametric study from FFD simulations to support optimal operation of the cooling system. First, we propose the thermal requirements regarding the three metrics (i.e. RCI_{LO}, RCI_{HI} and T_{in}^{max}). Then we identify possible settings of studied parameters that meet proposed thermal requirements based on the results of the parametric study in Section 4.2. Finally, we optimize and update the setpoints for studied parameters to achieve a minimum energy consumption for each month.

4.3.1 Evaluation metrics

In this case, two parameters including setpoints of supply air temperature and flow rate (air ratio) are optimized to achieve a minimum energy consumption for each month. The constraints include the ranges of two optimization variables and the thermal requirements regarding the three metrics (i.e. T_{in}^{max}, RCI_{LO}, RCI_{HI}). The two optimization variables are discrete variables and the search spaces are based on values of two studied parameters defined in

. The requirements for the three metrics vary for different cases and are defined in Table 6.

$$\min_{T_{sup},\dot{m}_{sup}} \sum_{i=0}^{N} \int_{t_1}^{t_2} E_i, \tag{23}$$

s.t. $T_{sup}^{(min)} \leq T_{sup} \leq T_{sup}^{(max)}$

$\dot{m}_{sup}^{(min)} \leq \dot{m}_{sup} \leq \dot{m}_{sup}^{(max)}$

$T_{in}^{max} \leq T_{in}^{max(required)}$

$RCI_{LO} \leq RCI_{LO}^{(required)}$

$RCI_{HI} \leq RCI_{HI}^{(required)}$

where, E_i is the energy consumption of cooling system component i. N is the number of cooling system components. T_{sup} and $\dot{m}_{sup}$ are the supply air temperature and mass flow rate. t_1 and t_2 are the start time and end time of each month.

4.3.2 Setup of the case

Three cases are proposed with different thermal requirements as shown in Table 6. In the baseline, T_{in}^{max} is 2 °C lower than ASHRAE recommended upper limit (27 °C) and all rack inlet temperatures are within recommended range (18-27 °C). The proposed Case 1 has the same thermal requirement as the baseline. Case 2 and 3 are proposed to investigate the energy saving potentials while sacrificing thermal environment compared to the baseline but still meeting the requirements of standards.

The energy performance is evaluated from energy simulations based on a detailed physics-based cooling system model in Modelica. The cooling system model was developed and validated in our previous work [50]. The cooling system features a chilled water system with airside economizers

(ASEs), which provides free cooling in cold weather. The cooling system operates in three cooling modes: (1) free cooling (FC) mode, where only ASEs are activated; (2) partial mechanical cooling (PMC) mode, where the chilled water system and ASEs work simultaneously; (3) fully mechanical cooling (FMC) mode, where only the chilled water system is used. The transition conditions between cooling modes are determined based on the weather data, system settings and conditions. For example, the FC mode switches to PMC mode when the outdoor dry bulb temperature is higher than the raised-floor plenum temperature setpoint (which determines supply air temperature) plus a dead band and the outdoor dew point temperature is higher than its predefined low cutoff limit plus a dead band. For more detailed description of the cooling system, please refer to Fu, et al. [50].

Table 6 Baseline and proposed cases that meet different thermal requirements

Cases	**Thermal Requirements**			**Notes [24]**
	T_{in}^{max}	RCI_{LO}	RCI_{HI}	
Baseline	$= 25℃$	$= 1.0$	$= 1.0$	• T_{in}^{max} is 2 °C lower than ASHRAE recommended upper limit (27 °C) and all rack inlet temperatures are within ASHRAE recommended range (18-27 °C).
Case 1	$\leq 25℃$	$= 1.0$	$= 1.0$	• T_{in}^{max} is no higher than that in baseline and all rack inlet temperatures are within ASHRAE recommended range (18-27 °C).
Case 2	$\leq 27℃$	$= 1.0$	$= 1.0$	• T_{in}^{max} is no higher than ASHRAE recommended upper limit (27 °C) and all rack inlet temperatures are within ASHRAE recommended range (18-27 °C).
Case 3	$\leq 35℃$	≥ 0.96	≥ 0.96	• T_{in}^{max} is no higher than ASHRAE allowable upper limit (35 °C) and most rack inlet temperatures are within ASHRAE recommended range (18-27 °C).

4.3.3 Results

As shown in Figure 16, candidate selections of air ratio and supply air temperature are determined according to the results of the parametric study and the thermal requirements of Cases 1-3 described in Table 6. Generally, the supply air temperature is lower when the air ratio is smaller to avoid the generation of hot spots and higher when the air ratio is larger to avoid over-cooling (i.e. rack inlet temperature is lower than recommended lower limit).

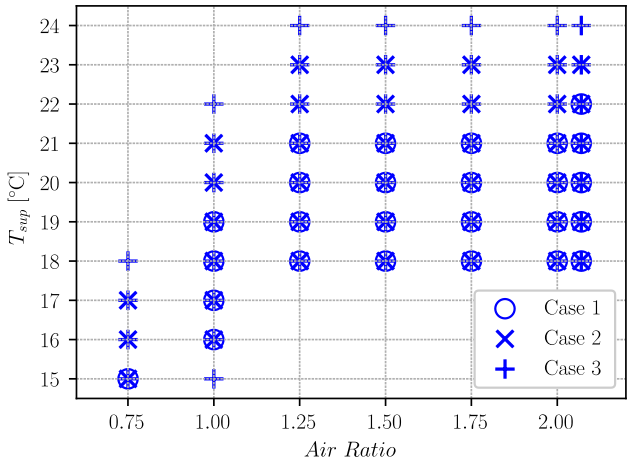

Figure 16 Candidate selections of air ratio and supply air temperature that meet different thermal requirements for Cases 1-3

To achieve optimal operation for Cases 1-3, the setpoints of air ratio and supply air temperature are optimized for each month using an exhaustive search among the searching space defined in Figure 16. The results are shown in Figure 17. The baseline, in which air ratio is set as 2.07 and supply air temperature is set as 22 ºC unvaryingly throughout the year, consumes the highest amount of energy. Among the proposed three cases, Case 1 with the strictest thermal requirement is the least energy efficient while Case 3 with the minimum thermal requirement is the most energy efficient. In Case 1, the energy consumption is reduced by decreasing the air ratio and lowering the supply air temperature. Consequently, the fan energy decreases and chiller energy increases. This results in an overall energy decrease as the fan energy is dominant throughout the year. Compared to Case 1, Cases 2 and 3 achieve higher energy savings of a wider range of allowable supply air temperature for each air ratio.

For the three proposed cases, the monthly optimal settings of the air ratio and supply air temperature are determined based on different weather profiles in each month. In cold months including January to May, November and December, the cooling system operates on FC mode mostly and the fan energy is dominant in the total energy consumption. As a result, the optimal setting of the air ratio adopts the minimum value and the setting of supply air temperature has little impact on the energy. In hot months from June to October, the optimal setting of the supply air temperature tends to adopt a higher value to get more free cooling. However, this usually requires a higher air ratio to meet the thermal requirement, which consequently leads to more fan energy consumption. As a result, there is a trade-off between saving the chiller energy and fan energy through adjusting the supply air temperature and air ratio. To conclude, through adjusting the settings of air ratio and supply air temperature for each month, Cases 1-3 reduce the annual energy consumption by 139.8 MWh (53.4%), 149.5 MWh (57.1%) and 153.7 MWh (58.8%) from the baseline (261.6 MWh), respectively, while still meeting the thermal requirements.

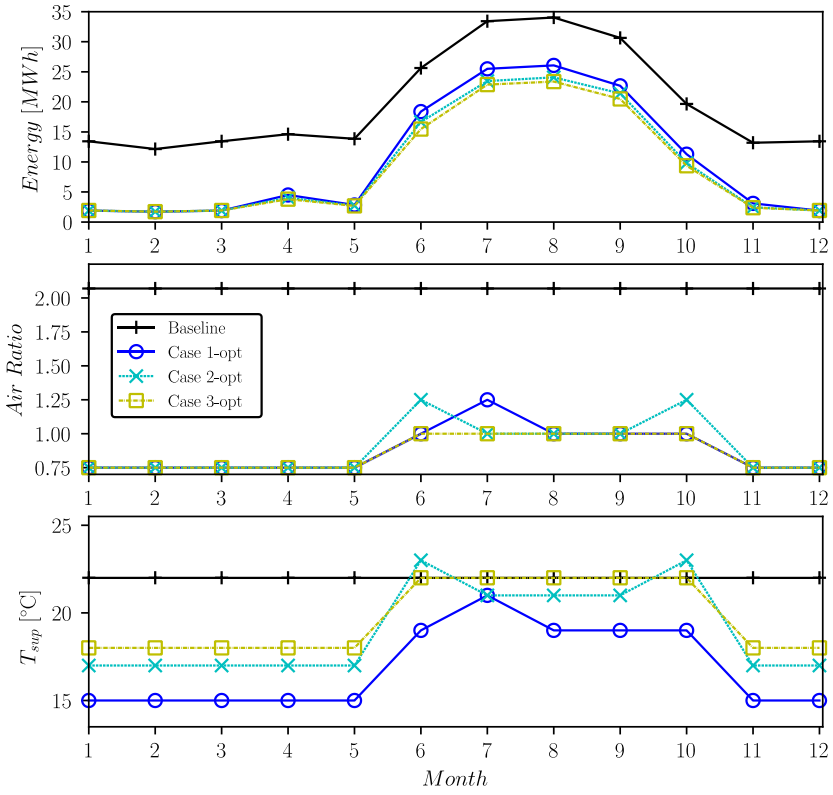

Figure 17 Energy consumptions and optimal settings of the cooling system for baseline and Cases 1-3

5 Discussions

5.1 Accuracy and Speed of the FFD model

In the validation with two indoor environment cases, the FFD model does not predict the velocity at the areas close to the ceiling and floor precisely. In addition to lack of wall functions in the FFD model, the prediction performance at near-boundary areas may also be influenced by configurations of the mesh and settings of physical parameters. When the turbulent viscosity is estimated improperly, it may lead to improper prediction of the near-wall airflow and further influence the overall prediction performance. Hence, future research is needed to improve the prediction performance at near-boundary areas with the FFD model.

For the data center case, the FFD results are not perfectly consistent with the experimentally measured data. This may be due to various reasons. One possible reason is that there is some physical information (e.g. leakage through tile gap, cables or other obstacles in the plenum) at some local areas that the simulation models fail to capture. Another possible explanation is that the measurements are carried out over a period of hours, during which the airflow and temperature may vary because of control dynamics of the cooling system. Since the scope of this paper is to

evaluate the possibilities to use the FFD model for data center thermal management, the validation results of FFD are acceptable since the proposed FFD achieves a similar level of accuracy compared to CFD. Note that the FFD model was originally applied to predict indoor environment with the purpose of fast speed. Even though it showed great success in different applications [16, 18, 26, 27], the FFD model may not be suitable for applications that require strictly high accuracy without further improvements.

For the computational speed, the FFD model running on GPU is approximately 61 times faster than CFD running on a CPU with four cores. It is noted that the computing time obtained in Section 3.2.4 is highly associated with the computer configurations and convergence parameters, which are case-by-case. Even so, for the case we studied, the 61 times of the speed significantly reduces the computing time of the case study in Section 4. The total computing time of the parametric studies is about 7.6 hours, which is estimated to be 464.8 hours if CFD is used. The improvement from about 20 days to several hours makes model-based design and operation more feasible and practical.

5.2 Potential Applications using the FFD model

The FFD model is promising for applications with high computing demand due to its significant speedup compared to CFD. One application is optimal design of data centers, especially when multiple parameters should be considered in the early design stage, which requires lots of simulations. Another application is optimal operation of data centers. Except for the case we demonstrate in Section 4.3, when thermal management and energy efficiency of the cooling system are simultaneously considered, a data-driven model may be adopted to predict critical information of thermal environment since the physics-based model is not fast enough for real-time optimal control. If synthetic data is needed to train the data-driven model, FFD can accelerate this process by providing a dataset much faster than CFD does.

5.3 Future Work

The future work may include the following directions. First, more complex component models can be adopted in the FFD model to predict the complex data center thermal environment. This may impose negative influence on the speed and its necessity depends on the requirements of applications. Second, a few improvement can be made to further accelerate the speed, such as optimizing the OpenCL codes and employing different discretization and solving methods. In addition, the prediction accuracy of the FFD model can also be improved by adopting more complex turbulence models and wall functions.

Another area of further work could be simultaneously modeling the plenum and white space since these two are modeled separately in our current FFD model. There are generally two approaches to achieve that. The first is a co-simulation-based approach where the white space and plenum are simulated separately in parallel. At each time step of the two simulations, data is exchanged

between the two simulations. For example, the airflow rates at perforated tiles calculated in plenum model are sent to the white space model, and the pressure distributions above the floor tiles calculated in the whitespace model are sent to the plenum model. The two simulations will be processed until both converge. The other option is an integrated approach, in which the white space and plenum are modeled as one space, and the perforated tiles are modeled as resistances in the Navier Stokes equation. The treatment of the perforated tiles will be different in this approach. Instead of inlets or outlets, the perforated tiles will be treated as momentum sources within the modeling space.

6 Conclusion

The new FFD model is first introduced including governing equations, new methods to solve these equations, treatments of special boundary conditions in data centers and the implementation. The new model is then validated with two classical cases for indoor environment modeling and the results show that it achieves better accuracy and faster speed compared to conventional FFD. It is also observed that both FFD models achieve acceptable accuracy, except for a few localized disparities with experimental data, which might be due to simplified handling of turbulent viscosity near the boundaries. It is also validated with a real medium-size raised-floor data center located in Massachusetts, U.S.A. The results show that the proposed FFD model running on GPU can achieve a similar level of accuracy while being much faster compared to a CFD model running on a CPU with four cores for the studied case. It is worthy to note that some discrepancies between simulation and measurement can still be observed in the data center case. This is acceptable given that the scope of this paper is to develop an open source, adequate and fast alternative to CFD. Subsequently, the FFD model is demonstrated to optimize the design of data center plenum and perforated floor tiles as well as the design of the cooling system through parametric studies. Quantified results are obtained regarding the effect of perforated tile open-area-ratio and plenum depth on the uniformity of airflow among perforated tiles and the effect of supply air temperature and flow rate on the cooling performance, which can be used to improve the design. Furthermore, the model-based optimal operation of the cooling system is explored by optimizing the setpoints of air ratio and supply air temperature for each month under three different thermal requirements. Depending on the thermal requirements of the data center, the proposed model-based optimal operation could offer annual energy savings from 53.4% to 58.8%.

With a much faster speed than traditional CFD, the FFD model is promising for carrying out practical model-based design and operation to improve data center thermal management. Even so, future work is still needed to continue to improve the speed for applications such as on-line optimal control. In addition, the prediction accuracy of the FFD model can also be improved by adopting more advanced turbulence models.

7 Acknowledgment

This material is based upon work supported by the U.S. Department of Energy's Office of Energy Efficiency and Renewable Energy (EERE) under the Award Number DE-0007688. This work emerged from the IBPSA Project 1, an international project conducted under the umbrella of the International Building Performance Simulation Association (IBPSA). Project 1 will develop and demonstrate a BIM/GIS and Modelica Framework for building and community energy system design and operation.

8 Disclaimer

9 Reference

[1] A. Shehabi, S. Smith, D. Sartor, R. Brown, M. Herrlin, J. Koomey, E. Masanet, N. Horner, I. Azevedo, W. Lintner, United states data center energy usage report, (2016).

[2] M. Salim, R. Tozer, Data Centers' Energy Auditing and Benchmarking-Progress Update, ASHRAE transactions, 116 (1) (2010).

[3] T. Evans, The Different Technologies for Cooling Data Centers White Paper 59 Version 2, in, Schneider Electric's Data Center Science Center, 2012.

[4] A. Capozzoli, G. Primiceri, Cooling systems in data centers: state of art and emerging technologies, Energy Procedia, 83 (2015) 484-493.

[5] J. Rambo, Y. Joshi, Modeling of data center airflow and heat transfer: State of the art and future trends, Distributed and Parallel Databases, 21 (2-3) (2007) 193-225.

[6] S.V. Patankar, Airflow and cooling in a data center, Journal of Heat transfer, 132 (7) (2010) 073001.

[7] J.W. VanGilder, R.R. Schmidt, Airflow uniformity through perforated tiles in a raised-floor data center, in: ASME 2005 Pacific Rim Technical Conference and Exhibition on Integration and

Packaging of MEMS, NEMS, and Electronic Systems collocated with the ASME 2005 Heat Transfer Summer Conference, American Society of Mechanical Engineers, 2005, pp. 493-501.

[8] C.M. Healey, J.W. VanGilder, Z.R. Sheffer, X.S. Zhang, Potential-Flow Modeling for Data Center Applications, in: ASME 2011 Pacific Rim technical conference and exhibition on packaging and integration of electronic and photonic systems, American Society of Mechanical Engineers Digital Collection, 2011, pp. 527-534.

[9] Q. Tang, T. Mukherjee, S.K. Gupta, P. Cayton, Sensor-based fast thermal evaluation model for energy efficient high-performance datacenters, in: 2006 Fourth International Conference on Intelligent Sensing and Information Processing, IEEE, 2006, pp. 203-208.

[10] Z. Song, B.T. Murray, B. Sammakia, Multivariate prediction of airflow and temperature distributions using artificial neural networks, in: ASME 2011 Pacific Rim Technical Conference and Exhibition on Packaging and Integration of Electronic and Photonic Systems, American Society of Mechanical Engineers Digital Collection, 2011, pp. 595-604.

[11] B. Elhadidi, H.E. Khalifa, Application of Proper Orthogonal Decomposition to Indoor Airflows, ASHRAE Transactions, 111 (1) (2005).

[12] C.M. Healey, J.W. VanGilder, Z.M. Pardey, Perforated Tile Airflow Prediction: A Comparison of RANS CFD, Fast Fluid Dynamics, and Potential Flow Modeling, in: ASME 2015 International Technical Conference and Exhibition on Packaging and Integration of Electronic and Photonic Microsystems collocated with the ASME 2015 13th International Conference on Nanochannels, Microchannels, and Minichannels, American Society of Mechanical Engineers, 2015, pp. V001T009A024-V001T009A024.

[13] S. Patankar, Numerical heat transfer and fluid flow, CRC press, 1980.

[14] W. Zuo, Q. Chen, Fast and informative flow simulations in a building by using fast fluid dynamics model on graphics processing unit, Building and Environment, 45 (3) (2010) 747-757.

[15] W. Zuo, Q. Chen, Real-time or faster-than-real-time simulation of airflow in buildings, Indoor air, 19 1 (2009) 33-44.

[16] W. Zuo, Q. Chen, Validation of fast fluid dynamics for room airflow, in: IBPSA Building Simulation 2007, 2007.

[17] W. Tian, T.A. Sevilla, W. Zuo, A systematic evaluation of accelerating indoor airflow simulations using cross-platform parallel computing, Journal of Building Performance Simulation, 10 (3) (2017) 243-255.

[18] M. Jin, W. Zuo, Q. Chen, Simulating natural ventilation in and around buildings by fast fluid dynamics, Numerical Heat Transfer, Part A: Applications, 64 (4) (2013) 273-289.

[19] W. Liu, R. You, J. Zhang, Q. Chen, Development of a fast fluid dynamics-based adjoint method for the inverse design of indoor environments, Journal of Building Performance Simulation, 10 (3) (2017) 326-343.

[20] A. Katal, M. Mortezazadeh, L.L. Wang, Modeling building resilience against extreme weather by integrated CityFFD and CityBEM simulations, Applied Energy, 250 (2019) 1402-1417.

[21] W. Tian, J.W. VanGilder, X. Han, C.M. Healey, M.B. Condor, W. Zuo, A New Fast Fluid Dynamics Model for Data-Center Floor Plenums, ASHRAE Transactions, 125 (2019).

[22] W. Tian, J. VanGilder, M. Condor, X. Han, W. Zuo, An Accurate Fast Fluid Dynamics Model for Data Center Applications, in: 2019 18th IEEE Intersociety Conference on Thermal and Thermomechanical Phenomena in Electronic Systems (ITherm), IEEE, 2019, pp. 1275-1281.

[23] M. Wang, Q. Chen, Assessment of various turbulence models for transitional flows in an enclosed environment (RP-1271), Hvac&r Research, 15 (6) (2009) 1099-1119.

[24] ASHRAE, Data Center Power Equipment Thermal Guidelines and Best Practices, in, American Society of Heating, Refrigerating and Air-Conditioning Engineers, Atlanta, GA, 2016.

[25] M. Jin, Q. Chen, Improvement of fast fluid dynamics with a conservative semi-Lagrangian scheme, International Journal of Numerical Methods for Heat & Fluid Flow, (2015).

[26] W. Liu, M. Jin, C. Chen, R. You, Q. Chen, Implementation of a fast fluid dynamics model in OpenFOAM for simulating indoor airflow, Numerical Heat Transfer, Part A: Applications, 69 (7) (2016) 748-762.

[27] M. Mortezazadeh, L.L. Wang, Solving city and building microclimates by fast fluid dynamics with large timesteps and coarse meshes, Building and Environment, (2020) 106955.

[28] R. Courant, E. Isaacson, M. Rees, On the solution of nonlinear hyperbolic differential equations by finite differences, Communications on pure and applied mathematics, 5 (3) (1952) 243-255.

[29] A.J. Chorin, A numerical method for solving incompressible viscous flow problems, Journal of computational physics, 2 (1) (1967) 12-26.

[30] A. Staniforth, J. Côté, Semi-Lagrangian integration schemes for atmospheric models—A review, Monthly weather review, 119 (9) (1991) 2206-2223.

[31] M. Mortezazadeh, L. Wang, An adaptive time-stepping semi-Lagrangian method for incompressible flows, Numerical Heat Transfer, Part B: Fundamentals, 75 (1) (2019) 1-18.

[32] V.K. Arghode, Y. Joshi, Rapid modeling of air flow through perforated tiles in a raised floor data center, in: Fourteenth Intersociety Conference on Thermal and Thermomechanical Phenomena in Electronic Systems (ITherm), IEEE, 2014, pp. 1354-1365.

[33] E. Fried, I. Idelchik, Flow resistance, A Design Guide for Engineering, Hemisphere Publ, in, Co, 1989.

[34] W.A. Abdelmaksoud, T.Q. Dang, H.E. Khalifa, R.R. Schmidt, M. Iyengar, Perforated tile models for improving data center CFD simulation, in: 13th InterSociety Conference on Thermal and Thermomechanical Phenomena in Electronic Systems, IEEE, 2012, pp. 60-67.

[35] J.Z. Zhai, K.A. Hermansen, S. Al-Saadi, The Development of Simplified Rack Boundary Conditions for Numerical Data Center Models, ASHRAE Transactions, 118 (2) (2012).

[36] X. Zhang, J.W. VanGilder, M. Iyengar, R.R. Schmidt, Effect of rack modeling detail on the numerical results of a data center test cell, in: 2008 11th Intersociety Conference on Thermal and Thermomechanical Phenomena in Electronic Systems, IEEE, 2008, pp. 1183-1190.

[37] Z.M. Pardey, J.W. VanGilder, C.M. Healey, D.W. Plamondon, Creating a calibrated CFD model of a midsize data center, in: ASME 2015 International Technical Conference and Exhibition on Packaging and Integration of Electronic and Photonic Microsystems collocated with the ASME 2015 13th International Conference on Nanochannels, Microchannels, and Minichannels, American Society of Mechanical Engineers, 2015, pp. V001T009A029-V001T009A029.

[38] R. Schmidt, E. Cruz, Cluster of high-powered racks within a raised-floor computer data center: Effect of perforated tile flow distribution on rack inlet air temperatures, J. Electron. Packag., 126 (4) (2004) 510-518.

[39] X. Han, W. Tian, J.W. VanGilder, M. Condor, W. Zuo, doetools, in, https://github.com/doetools/isat_ffd/releases, 2018.

[40] J.W. VanGilder, Z.R. Sheffer, X.S. Zhang, C.M. Healey, Potential Flow Model for Predicting Perforated Tile Airflow in Data Centers, ASHRAE Transactions, 117 (2) (2011).

[41] Q. Chen, W. Xu, A zero-equation turbulence model for indoor airflow simulation, Energy and buildings, 28 (2) (1998) 137-144.

[42] P. Dhoot, J. VanGilder, Z. Pardey, C. Healey, Zero-Equation Turbulence Models for Large Electrical and Electronics Enclosure Applications, in: Proceedings of 2017 ASHRAE Winter Conference, 2017.

[43] M. Jin, W. Zuo, Q. Chen, Improvements of fast fluid dynamics for simulating air flow in buildings, Numerical Heat Transfer, Part B: Fundamentals, 62 (6) (2012) 419-438.

[44] J.W. VanGilder, Z.M. Pardey, C. Healey, Measurement of perforated tile airflow in data centers, ASHRAE Transactions, 122 (2016) 88.

[45] J.W. VanGilder, X.S. Zhang, Coarse-grid CFD: The effect of grid size on data center modeling, ASHRAE Transactions, 114 (2008) 166.

[46] M.K. Herrlin, Rack cooling effectiveness in data centers and telecom central offices: The rack cooling index (RCI), Transactions-American Society of Heating Refrigerating and Air conditioning Engineers, 111 (2) (2005) 725.

[47] M.K. Herrlin, Improved data center energy efficiency and thermal performance by advanced airflow analysis, in: Proceedings of Digital Power Forum, 2007, pp. 10-12.

[48] R. Sharma, C. Bash, C. Patel, Dimensionless parameters for evaluation of thermal design and performance of large-scale data centers, in: 8th AIAA/ASME Joint Thermophysics and Heat Transfer Conference, 2002, pp. 3091.

[49] J.W. Vangilder, S.K. Shrivastava, Capture Index: An Airflow-Based Rack Cooling Performance Metric, ASHRAE transactions, 113 (2007) 126.

[50] Y. Fu, W. Zuo, M. Wetter, J.W. VanGilder, X. Han, D. Plamondon, Equation-based object-oriented modeling and simulation for data center cooling: A case study, Energy and Buildings, 186 (2019) 108-125.